CHARACTERIZATION, SHAPING, AND JOINING OF SiC/SUPERALLOY SHEET FOR EXHAUST SYSTEM COMPONENTS

J. A. Cornie

July 20, 1977
Final Report

NASA CR-135301
Contract NAS-19735

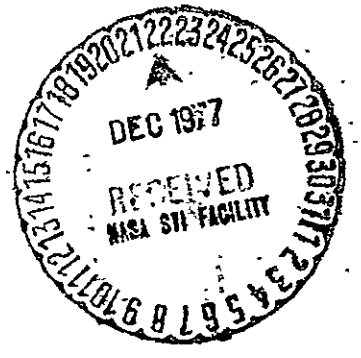

Westinghouse R&D Center
1310 Beulah Road
Pittsburgh, Pennsylvania 15235

NASA CR-135301
9D4-NASIC-R1

CHARACTERIZATION, SHAPING, AND JOINING OF SiC/SUPERALLOY SHEET FOR EXHAUST SYSTEM COMPONENTS

by J. A. Cornie

WESTINGHOUSE RESEARCH AND DEVELOPMENT CENTER

prepared for

NATIONAL AERONAUTICS AND SPACE ADMINISTRATION

NASA Lewis Research Center
Contract NAS-19735

1. Report No.	2. Government Accession No.	3 Recipient's Catalog No
NASA CR-135301		

4 Title and Subtitle	5. Report Date
CHARACTERIZATION, SHAPING, AND JOINING OF SiC/SUPERALLOY SHEET FOR EXHAUST SYSTEM COMPONENTS	July 1977
	6. Performing Organization Code
7. Author(s)	8. Performing Organization Report No.
J. A. Cornie	
	10. Work Unit No.
9 Performing Organization Name and Address	
Westinghouse Research & Development Center 1310 Beulah Road Pittsburgh, PA 15235	11. Contract or Grant No NAS3-19735
	13. Type of Report and Period Covered
12. Sponsoring Agency Name and Address	Contractor Report
Lewis Research Center	14. Sponsoring Agency Code

15. Supplementary Notes

16. Abstract

Hafnium carbide was shown to be virtually inert when in contact with silicon carbide and Waspaloy for at least 200 hr at 1093°C (2000°F). Extensive interaction was noted with other superalloys such as HA-188. A continuous CVD HfC deposition process was developed for deposition of up to 8 μm on .14 mm (.0056") SiC tungsten core filament at rates as high as .6 m/min. The rate can be increased by increasing the length of the reactor and the output of the power supply used in resistive heating of the filament substrate.

The strength of HfC coated filament varies with thickness in a Griffith-like manner. This strength reduction was greater for HfC coatings than for tungsten coatings, presumably because of the greater ductility of tungsten. Satisfactory composite strengths were not obtained for a variety of identifiable reasons which are discussed. Room temperature modulus values measured were only slightly below rule-of-mixture predictions.

17. Key Words (Suggested by Author(s))	18 Distribution Statement
Composites Metal Matrix Diffusion Barriers Silicon Carbide Hafnium Carbide Hot Isostatic Pressing Waspaloy Compatibility	Unclassified - Unlimited

19. Security Classif. (of this report)	20. Security Classif. (of this page)	21. No. of Pages	22. Price*
Unclassified	Unclassified	87	

* For sale by the National Technical Information Service, Springfield, Virginia 22161

TABLE OF CONTENTS

FOREWORD

This technical report describes work performed for NASA-Lewis Research Center under Contract NAS3-19735 during the period January 1975 to April 30, 1977. It was submitted by the authors in July 1977. The contract with the Metallurgy and Metals Processing Department of Westinghouse Research and Development Center, Westinghouse Electric Corporation, Pittsburgh, PA 15235, was under the direction of Dr. Richard Barrows of the NASA-Lewis Research Center, Cleveland, OH.

Westinghouse personnel contributing to this program are: Dr. J. A. Cornie, Program Manager, Mr. J. W. Salatka and W. R. Lovic, Composite Fabrication, Hot Isostatic Pressing, and Filament Testing, G. A. Blann, Metallography, and E. Diaz, Composite Testing.

ABSTRACT

Hafnium carbide was shown to be virtually inert when in contact with silicon carbide and Waspaloy for at least 200 hr at 1093°C (2000°F). Extensive interaction was noted with other superalloys such as HA-188. A continuous CVD HfC deposition process was developed for deposition of up to 8 μm on .14 mm (.0056") SiC tungsten core filament at rates as high as .6 m/min. The rate can be increased by increasing the length of the reactor and the output of the power supply used in resistive heating of the filament substrate.

The strength of HfC coated filament varies with thickness in a Griffith-like manner. This strength reduction was greater for HfC coatings than for tungsten coatings, presumably because of the greater ductility of tungsten. Satisfactory composite strengths were not obtained for a variety of identifiable reasons which are discussed. Room temperature modulus values measured were only slightly below rule-of-mixture predictions.

ACKNOWLEDGEMENT

The technical assistance of the following individuals is gratefully acknowledged: I Ahamad of Watervliet Arsenal for providing CVD tungsten coated SiC filament, J. Hakim and P. Mazzei for developing a CVD apparatus and provess for continuous CVD coating of HfC onto SiC filaments, R. Lovic for HIP and Composite Fabrication assistance, D. Kaminski for designing the filament winding apparatus, J. Salatka for encapsulation development, and G. Blann for developing metallographic techniques for SiC reinforced superalloys.

1. INTRODUCTION

The work on the previous contract (NAS3-18921) demonstrated that SiC filament could be fabricated at temperatures as low as 996°C (1825°F) if adequate protection against interdiffusion between matrix and fiber is provided. This protection can be in the form of a diffusion barrier applied to the filament surface prior to composite consolidation. Tungsten was used as the barrier with some success but more notable drawbacks. Tungsten increases the composite density and delays, but does not prevent the decomposition of the filament through interaction with matrix constituents.

A considerable amount of effort has been necessary to develop better barriers. Fortunately, candidates with a high probability of success were investigated during earlier studies.[1] Hafnium carbide was shown to be virtually inert to interaction between SiC and the Waspaloy matrix and was selected as the barrier material. A Chemical Vapor Deposition (CVD) method was developed for continuously coating the SiC filament with HfC.

Fabrication techniques were developed utilizing matrix in the form of a powder tape sandwiched between monolayers of fiber in the desired orientation. Consolidation was accomplished by Hot Isostatically Pressing (HIP) after removal of the fugitive binder in the powder tape. Although the processing parameters were established during the previous program, much work still remained for process refinement and optimization. This work was continued under the present program.

A further objective of this program was the characterization of mechanical properties of the resultant composites as a function of thermal exposure at 982°C (1800°F).

The reader is referred to Reference 2 for the description and qualification of initial matrix materials.

2. COMPATIBILITY

Silicon carbide and any Ni, Co, or Fe base superalloy are inherently incompatible. This was dramatically demonstrated in the previous program (Contract NAS3-18921).[2] Any attempt to circumvent the compatibility problem through alloy modifications would meet with failure. Although kinetics of the complex intermetallics can be affected somewhat, the laws of thermodynamics remain inviolate. A typical example of chemical interaction between SiC filament and superalloy matrices is shown in Fig. 1.

In order to prevent interaction between the filament and matrix, physical separation is necessary, in effect, a diffusion barrier. 1) The essential features of a good diffusion barrier are: (1) high temperature stability, (2) chemical compatibility with both the matrix and with the filament, and (3) mechanical compatibility with the fiber/matrix interface (thermal expansion match). Item 1 above is related to the melting point of the barrier. Refractory materials such as oxides, carbides, certain nitrides, and tungsten metal would be good candidates. Item 2 is related to the free energy of formation of candidate materials. Item 3 is related to the thermal expansion mismatch.

During earlier work at this laboratory, a similar problem (however with less disasterous consequences) was encountered when attempting to induce high temperature stability in tungsten/superalloy composites.[1]

A number of candidate materials are compared for free energy of formation and thermal expansion mismatch in Table 1. Chemical potential vs temperature plots for selected carbides and oxides are given in Figs. 2 and 3, respectively. From free energy of formation

TABLE 1

THERMAL AND CHEMICAL STABILITY DATA

Species	Thermal Expansion Coefficient $\alpha \times 10^6/°C$	Temp. Range, °C	$-\Delta G_{1500°K}$ kcal
Fiber			
W	4.6	20 → 2000	
SiC	4.78	20 → 1250	11.7
Matrix			
Waspalloy	12.8	20 → 204	--
	13.7	20 → 426	
	14.4	20 → 650	
	16.0	20 → 870	
	18.7	20 → 1093	
Carbides			
TiC	7.74	20 → 270	39
ZrC	6.73	20 → 1100	43
HfC	6.59	20 → 600	47
.aC	6.29	20 → 1100	.34
WC	3.84	20 → 400	8
Oxides			
Al_2O_3	9.0	20 → 982	202
Y_2O_3	8.5	20 → 1093	207
TiO_2	4.9	20 → 1093	160
ZrO_2	7.9	20 → 1093	197
HfO_2	5.6	20 → 1093	204
Cr_2O_3	6.9	20 → 1093	108
Nitrides			
TiN	8.1	20 → 600	47
	9.0	600 → 1400	
ZrN	7.0	20 → 600	53
	7.7	600 → 1400	
HfN	6.5	20 → 1400	~56

considerations alone, HfC would be the most stable carbide, HfN the most stable nitride, and Al_2O_3, Y_2O_3, and HfO_2 being equally promising as oxide barriers.

During the earlier study,[1] a number of the candidate barrier compounds were applied to tungsten wire by R. F. sputtering, and wires were enclosed in Mar-M-200 powder and HIP consolidated at 1020°C into compatibility specimens. The diffusion of Ni through the various barriers into the tungsten wire substrate as manifested by Ni enhanced recrystallization[3-5] of the outer layers of the tungsten wire is shown in Fig. 4 for the 1177°C (2150°F) isotherm. Hafnium carbide far surpassed the other carbides. Hafnium nitride was not investigated at the time of the work in Ref. 1. Later work[6] has also shown HfN to be a very stable barrier. However, due to the extreme range of nitrogen solubility in the HfN structure, stoichiometry, i.e., the Hf/N ratio, is expected to have a large effect on the diffusivity of Ni through HfN.

Tungsten and HfC were selected during the previous work on NAS3-18921 as the most promising barriers for protecting SiC from reaction with the Waspaloy matrix. Tungsten, however, forms intermetallics with both sides of the interface. This is best demonstrated by observing the progressive interaction between the tungsten and the SiC at the core, as shown in Fig. 5. This interaction greatly reduces the strength of the filament. Tungsten forms intermetallic compounds with matrix constituents on the matrix/barrier interface, as shown in Fig. 6. The kinetics of growth of this compound at 982°C (1800°F) is given in Fig. 7. The intermetallic compounds continue to grow until the tungsten is completely consumed. The intermetallics, when in contact with the SiC filament, are unstable and a number of reaction products between SiC and the intermetallic compound are observed. Tungsten would be an adequate diffusion retardant, however, thicker tungsten layers would result in a density penalty as shown below.

Thickness W Coating μm	50 v/o Composite Density, g/cc	Density Penalty %
0	5.7	0
2	6	5.5
5	6.3	10.3
10	7.4	29.3

A 1000 hr life specification would require approximately a 10 μm coating. Most of the density advantage from using SiC reinforcement in a superalloy composite would be lost with a 10 μm barrier.

Hafnium carbide is the most promising barrier candidate for the intended composite application. Work on the present contract was directed toward developing a technique for HfC deposition and for verifying the effectiveness of HfC as a barrier.

It was still necessary to verify the stability of HfC when in contact with SiC and to assess the compatibility between HfC and the various superalloy candidates from the previous contract (NAS3-18921).

Slices of hot-pressed SiC were RF sputter deposited with HfC and HIP consolidated at 138 MPa (20 ksi), 996°C (1825°F) with Waspaloy, HA-188 and Hastelloy X powders into compatibility specimens. The couples were examined as HIP-consolidated and after thermal exposure at 982°C (1800°F) for 200 hr. The resulting optical micrographs are shown in Figs. 8, 9, and 10. The 12 μm thick HfC barrier prevented interdiffusion during the conditions investigated. However, some small interaction between the matrix and the HfC occurred after 200 hr at 982°C for the HA-188 and Hastelloy X/HfC/SiC couples and are shown in Figs. 12 and 13. No interaction was noted between the HfC and the Waspaloy matrix after 200 hr at 982°C, as shown in Figs. 8 and 11. Another encouraging result of this investigation was the lack of observable interaction between HfC and SiC.

Since very little reaction was noted at 982°C (1800°F) for any of the diffusion couples, accelerated tests were conducted at 1093°C (2000°F) to evaluate the margin of error in fabrication or application of SiC/superalloy composites. An Energy Dispersion X-ray (EDX) analysis

of the 10 hr at 1093°C Waspaloy/HfC/SiC couple is given in Fig. 14. The SEM photomicrographs revealed no microstructural changes resulting from the high temperature exposure. Slight amounts of Ti, Cr, Fe, and Co were detected in the barrier. Very little change in microstructure was noted in the Waspaloy/HfC/SiC couple after a 200 hr at 1093°C exposure, as shown in Fig. 15. The area shown in Fig. 15 was taken from the end of the wafer and received HfC during the total period of deposition. The two layers within the barrier are due to the interruption of the HfC sputter coating operation due to flipping the wafers over for total coverage. A thin intermediate phase between the Waspaloy matrix and the HfC coating is noted in Fig. 15. The EDX analysis shows this phase to be enriched in Ti and Mo with respect to the matrix and somewhat depleted in Cr, Fe, Co, and Ni. The barrier shows about the same degree of impurities after 200 hr as it did after 10 hr at 1093°C with the exception of a slightly higher Ni content (~130 counts after 200 hr vs no counts after 10 hr). All in all, this specimen displays a remarkable lack of interaction.

A somewhat greater interaction was noted between the constituents of the Hastelloy X/HfC/SiC couple after the 200 hr at 1093°C exposure of Fig. 16. A pronounced intermetallic phase is noted at the matrix/HfC interface and a second reaction zone at the HfC/SiC interface. An EDX analysis of the various features of this couple is also given in Fig. 16. Area A gives the characteristic counts above background for the Hastelloy X matrix. The intermediated phase at the HfC/matrix interface (spot B) shows a concentration of Mo with some Si, Cr, Fe, Co, and Ni. The barrier shows about the same level of impurities as the previous (Waspaloy/HfC/SiC) couple in Fig. 15 with the exception of a slightly higher Cr content. The exceptionally high Cr content in the intermediate zone between HfC and SiC was unexpected.

The H.A. 188/HfC/SiC couple was decidedly unstable after 200 h at 1093°C, as shown in Fig. 17. The initial barrier (area C) is much depleted, as shown by its porosity. At least one zone is shown between

the initial coating and the matrix and two zones between the matrix and SiC are noted in Fig. 17. This couple demonstrates the inadequacy of HA-188 as a matrix candidate with HfC barriers.

Our earlier choice of Waspaloy as the reference matrix has been vindicated by these experiments. We should expect excellent chemical stability from the Waspaloy/HfC/SiC system at 982°C (1800°F), the temperature of intended application. An opportunity to examine TiN coated SiC occurred when a CVD vendor* placed a filament into a reactor. The CVD TiN coated SiC filaments were HIP consolidated into Hastelloy X and Waspaloy powders. The photomicrographs of Figs. 18 and 19 revealed the presence of diffusion zones for both couples after the 2 hr HIP cycle at 996°C (1825°F). Energy dispersive X-ray analysis performed on the areas of the SEM indicated in Figs. 18 and 19 revealed matrix constituents concentrated in the inner zones. This amount of interdiffusion was considered excessive and TiN was eliminated as a barrier candidate.

Although TiN was inadequate as a diffusion barrier, HfN shows great promise. However, the amount of effort required to develop CVD HfN techniques was considered to be greater than CVD HfC techniques which had previously been developed for tungsten filament.

---

* Materials Technology Corporation, Dallas, TX.

3. FABRICATION AND PROCESSING

A. Filament Coating

With HfC established as a viable barrier for the SiC/Waspaloy system, the task remained to develop a process for depositing a high quality coating of the barrier continuously onto the SiC filament. Since hafniun is an expensive starting material, methods of developing high material efficiently must be identified. Chemical vapor deposition appeared to offer the best technique and can be scaled up to continuous production. Resistance heating of the substrate (filament) was selected as the most efficient technique for providing the hot surface for deposition with minimal process loss of hafnium.

The apparatus designed for the CVD or HfC for this program is shown in Fig. 20. $HfCl_4$ gas is generated by passing HCl vapor over heated hafnium chips. The $HfCl_4$ vapor is reduced and carburized simultaneously by the proper balance of CH_4 (methane) and hydrogen on the hot filament substrate. A record of the parametric studies conducted during the development phase of the program is given in Table 2. Once continuous production capability was reached, deposition of 5-8 μm HfC onto the SiC substrate was accomplished at approximately .6 m/min (2 ft/min).

B. Composite Panel Fabrication

Filament Winding. A filament winding apparatus was designed, consutructe, and placed into operation. The device shown in Fig. 21 attached to the tool bed of a 305 mm (12") lathe utilizes carriage feed gearing to provide the filament spacing required for a specific volume fraction. The filaments were tension-fed, by use of an infinitely adjustable magnetic brake shown on the spool axle of Fig. 21A, through a .38 mm (15 mil) diameter hole drilled axially through a Teflon cylinder (Fig. 21B) onto a 20 cm (8") diameter polished aluminum drum which was chucked and

TABLE 2. EXPERIMENTAL CVD PARAMETER STUDY FOR HfC DPEOSITION ON SiC FIBRE

Expt. No.	H_2 Cooling	H_2 Chlorination	H_2 Total	HCl $ml.min^{-1}$	CH_4 $ml.min^{-1}$	Speed inch min^{-1}	Power Setting Volts	Power Setting Amps	Remarks
CVD SiC-10 #1	50	100	150	10	-	2	700	0.75	Fibre darkens and is embrittled due probably to the direct reaction with Hf halides
#2	50	100	150	10	10	2.5	700	0.8	Spalling
#3	50	100	150	10	10	6	700	0.8	Spalling
#4	50	200	250	10	10	6	625	0.8	No spalling, sample to R&D
#5	50	200	250	10	10	12	700	0.5	No spalling, sample to R&D
CVD SiC-11 #1	100	200	300	10	10	12	705	0.8	Spalling
#2	100	300	400	10	10	9.5	705	0.8	No spalling, sample to R&D
#3	100	300	400	10	10	8	705	0.8	No spalling, sample to R&D
#4	100	300	400	10	20	12	705	0.5	Spalling
#5	100	400	500	10	12	12	705	0.5	No spalling, sample to R&D
#6	100	400	500	10	12	24	710	0.9	No spalling, sample to R&D
CVD SiC-12 #1	100	400	500	10	20	5	690	0.5	Spalling
#2	100	400	500	10	20	6	690	0.5	Spalling
#3	100	400	500	10	20	24	770	0.45	Spalling
#4	100	540	640	10	20	24	770	0.45	Spalling - a small portion of fibre showed good adhesion.
#5	100	100	200	10	20	24	770	0.45	No spalling, but temperature of SiC fibre went out of control.

--continued

Expt. No.	H_2			HCl	CH_4	Speed	Power Settings		Remarks
	Cooling	Chlorination	Total				Volts	Amps	
CVD SiC-13									
#1	100	175	275	5	10	4	660	0.35	Deposition rate very low
#2	100	175	275	5	10	4	700	0.4	No spalling
CVD SiC-14									
#2	100	100	200	4	10	12	650	0.5	Good quality adherent HfC coating (1.9 μm thick). About 100 ft. fibre coated of which 70 ft. used for laying down a duplex coating as in CVD SiC 15
CVD SiC-15									
#1	100	100	200	4	15	12	500	0.76	No spalling, HfC thickness= 3.2 μm, 60 ft. of fibre obtained.
#2	100	100	200	5	20	12	500	0.75	No spalling, HfC thickness= 3.3 μm.

NOTES:

(a) Hafnium metal was chlorinated at 700°C and walls of the CVD chamber were maintained at 450° - 500°C during a deposition run.

(b) Reference to the temperature of the fibre in the table has been omitted since a temperature gradient prevails along the length of the fibre during a deposition run due to large differences in the resistivities of SiC and HfC.

(c) Temperature of the fibre at the inlet end of the CVD chamber was made to vary between 950° & 1200°C, depending on the power setting, flow rates of gases and speed of travel of the fibre through the deposition chamber.

centered. The drum was first lined with a 25 μm thick Mylar film over which the powder tape is rolled and attached. Filament was then wound onto the powder tape surface at the desired pitch or spacing. The binder in the tape was softened by spraying with a mild solvent (Ethelyne Glycol Monobutyl Ether) which, after drying, results in the fiber being embedded into the powder tape. Heating with a hot air blower after winding produces the same result. The dried green monolayer was then cut by scoring along a premachined groove in the drum and unpeeled for stacking into picture frame HIP capsules.

Binder Removal and Panel Fabrication. The early test specimens and panels fabricated on this program were outgassed as an "open face sandwich", i.e., the ply-pattern was laid-up in the picture frame can and outgassed with flowing hydrogen by slowly heating to ∿450°C. After binder removal, the cover plate was then welded onto the green (but binder removed) lay-up and evacuated by electron beam closure. This method was advantageous because of the opportunity to inspect the lay-up for complete binder removal and because of the easy access of hydrogen to the binder and unrestricted flow for binder vaporization. However, the powder tape in the green composite stack is very friable, behaving much like a "clod of earth". During handling, some powder may shift or settle to certain areas in the capsule prior to HIP consolidation. Excessive shifting resulted in fiber breakage during HIP consolidation.

For the reasons given above, it was considered desirable to maintain a moderate compressive stress on the green composite lay-up during outgassing and handling. This compressive stress can best be provided by atmospheric pressure acting on the walls of a closed picture frame envelope during binder removal under a positive hydrogen flow at a reduced pressure. The capsule shown in Fig. 22 was utilized to remove the binder. The binder removal process was further modified by heating to 180-200°C and holding for 16 hr (overnight) then heating to 450°C at a rate of approximately 50°C/h followed by more rapid heating (∿150°C/hr) to 1000°C. This procedure insures total binder removal and hydrogen deoxidation.

of the powder surface. In addition, a small amount of sintering of the powder occurs and produces a more stable and less friable "green" compact.

Four small 2.54 x 15.2 cm (1" x 6") 4-ply uniaxial composites containing 50 v/o fiber were fabricated utilizing binder removal techniques and overall HIP can design discussed above. The object of these initial fabrication attempts was to evaluate several stacking arrangements and the use of parting compounds. The generalized stacking sequence is given below.

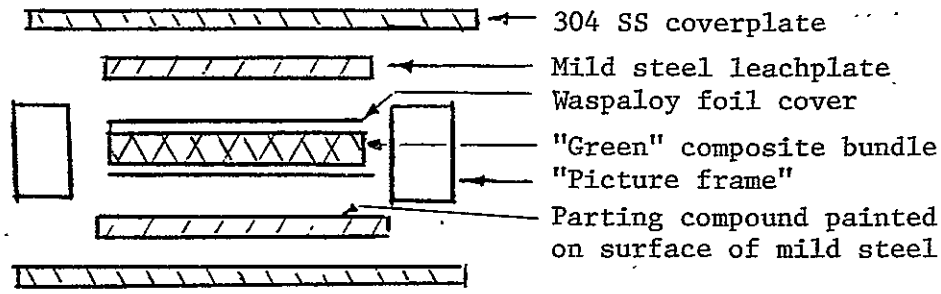

The parting compounds were boron nitride, graphite, and alumina painted onto the mild steel leaching plates in the form of an aqueous slurry.

The results of this fabrication experiment were decidedly unsatisfactory. The parting compound was too thin to provide a continuous friable layer and allowed diffusion bonding of the Waspaloy foil to the mild steel leachable inner can liner.

The second problem arose here due to thermal expansion differences between the composite and the HIP envelope. "Trouser Leg" tearing or delamination occurred after the end of the composite was exposed during leaching of the steel inner can. We would calculate, utilizing Schöberg's equation, an axial coefficient of thermal expansion for a uniaxial 50 v/o SiC/Waspaloy composite of 8.8×10^{-6} cm/cm/°C. The stainless steel and mild steel inner liner has an α of approximately 14 to 16×10^{-6} cm/cm/°C over the temperature range from RT to 1000°C. The resultant product is a double bimetallic strip as shown below. The

cladding contracts more than the composite during cooling, placing the composite in compression. Since the steel is diffusion bonded to the matrix, the residual stress is relieved by trouser-leg tearing as indicated below.

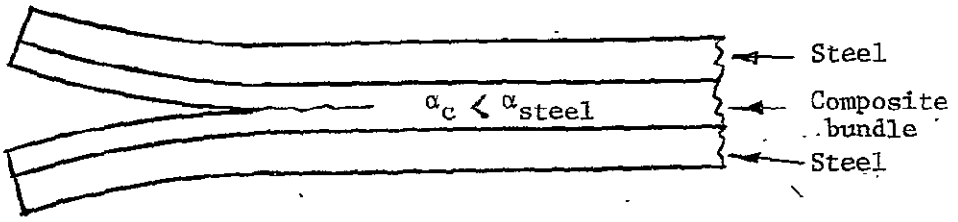

Fortunately, this problem has a solution. The delamination can be prevented by use of end clips and by use of an effective parting compound. These measures were taken on the next panel fabricated as shown in Fig. 23.

The fabrication sequence was altered by enclosing the green composite bundle in a tack welded box fabricated from .076 mm (.003") thick Waspaloy foil. "U" shaped Waspaloy end clips were inserted to seal the ends of the box and prevent delamination after HIP can removal. The box is prevented from bonding with the HIP envelope by surrounding with refractory insulating felt. During the hot isostatic pressing operation, the refractory felt densifies but prevents diffusion bonding between the Waspaloy of the composite and the 304 SS of the HIP envelope. The thermal stresses due to the expansion differences between the composite bundle and the envelope result in delamination within the original felt layer rather than within the composite. The action of the refractory felt is shown in Fig. 24 where the fibers become imbedded in the 304 SS cover sheet.

The successfully pressed panel (capsule #8S80-5 as disassembled after HIP consolidation) is shown in Fig. 25. Parts A and B are the top and bottom 304 SS covers of the HIP envelope and Part C is the composite panel. Delamination of the HIP capsule occurred spontaneously after the original picture frame was sliced away.

Examination of the HIP compact revealed no internal delamination. Fiber alignment remained excellent as shown in Fig. 26. The composite did have some defects, as shown in Figs. 27 and 28. There are several instances of fiber to fiber contact and occasional reaction blooms, presumably due to coating defects. A tungsten barrier layer was applied to the filament utilized in this particular panel. At higher magnification in Fig. 28, other defects related to hot isostatic pressing are noted. Item A occurs between fibers along a line perpendicular to the major compaction direction. Item D is a reaction bloom, C is a defect peculiar to the ductile tungsten barrier where the barrier plastically deforms and flows with the movement of matrix during consolidation. This flow may be one cause of the reaction blooms. The intensity of the flow is shown in the ovality of the previously spherical powder particles in areas between fibers oriented 45° to the consolidation direction, as shown in "B" type areas in Fig. 28.

A number of the composite panels were fabricated and delivered to the Government, as shown in Fig. 29. The strengths of these composites were inadequate, as will be discussed later. A closer evaluation of composite defects was required.

The most-obvious defect noted earlier in Fig. 28 was reaction blooms at coating defects. It was believed that the defects noted in Fig. 28 would be eliminated by application of a HfC barrier coating. This was not the case with the initial lot of developmental HfC coated SiC filament. Several explanations for the poor performance of the composite were considered, including chemical interaction through coating defects. It has been demonstrated (and will be discussed in the next section) that filament strength is lowered by the coating and handling steps in composite fabrication. However, the remaining fiber strength (given in the next section) is more than adequate to provide composite strengthening. We concluded that the strength deterioration must be related to the composite fabrication steps after the coating process.

It became necessary to examine the fibers in-situ to determine where the fiber deterioration was taking place. A section of as HIP consolidated composite panel was painted with Stoner-Mudge, an electrolytic resist lacquer. A small section (1 cm x 1/2 cm) was left unpainted and was electropolished in a 10% tartatic acid 7% HCl/methanol solution. The matrix was electrolytically removed until the first ply of the SiC filament was exposed, as shown in Fig. 30. A notable feature on the exposed filament surface are a number of tuberous growths or "blooms" indicating interaction between the matrix and SiC filament. The structure of these defects are shown clearly in the SEM photographs in Fig. 31. Additional surface features and energy dispersive X-ray spectra for selected areas are presented in Fig. 32. Area A contains every element present in the matrix in addition to Si. The Si comes from the interaction between Waspaloy and the filament. Other features from the unaffected surface show Hf from the HfC coating with perhaps some small amounts of matrix contamination.

The surface features and the X-ray analysis indicate that interaction occurred between the matrix and filament. The "blooms" are localized and only occur on certain filaments and not others. This leads us to conclude that coating imperfections allowed the interaction to occur. Further, we can see that the exposed filaments were not damaged by the fabrication process or HIP sequence as was originally feared.

The observation and location of a problem are the first steps to the solution. This program was not intended to be a coating development study. Yet, because of the reactivity between uncoated SiC and superalloys we were forced to divert a considerable effort into that direction at the expense of the fabrication and evaluation tasks. We can see that any realization of the inherent strength of SiC in a superalloy composite will be initially limited by the integrity of the barrier coating.

A number of fabrication related defects are shown in the radiographs of composite panels in Fig. 33. The mottled appearance represents nonuniformity of matrix distribution. Local movement of the powder apparently occurs during application of pressure during the HIP process. Panels A, E, and to some extent B show a thinning of matrix material near the circumference of the panels. In these cases, the matrix is actually extruded from between the filaments. Considerable change in fiber spacing and alignment occur as a result of this movement as shown in Figs. 34 and 35 which are micrographs taken from central and edge regions of a panel. Another feature seen in Fig. 33C is called "Mud Cracking" for lack of a better description, and presumably occurs as a result of too rapid binder removal. Bubbling of the binder also can cause local thinning of matrix powder, as seen in the speckled appearance of panel C and B. Microscopic examination of the radiograph shows some distortion of the filament near the thin spots.

The lateral matrix extrusion phenomenon can be corrected by tighter packing in the HIP envelope. The matrix powder will not extrude if properly confined.

Panel C (P-77-46) has a more uniform appearance than the other panels. This panel has 25 v/o reinforcement as compared to the 50 v/o in the other panels of Fig. 33.

In summary, fabrication defects appear to fall in the following categories:

1) Insufficient consolidation.
2) Coating flaws resulting in chemical interaction between the filament and matrix.
3) Matrix extrusion away from the composite during HIP.
4) Matrix distribution irregularities due to local movement during binder removal.

4. FILAMENT CHARACTERIZATION

The results of RT tensile tests of all of the various lots of tungsten core SiC received from the government are given in Table 3. A few of the better, more consistent materials and one lot of the poorest material were selected for tensile characterization at 982°C. The purpose of this evaluation was to screen the available material for fiber having adequate RT and 982°C strength and to characterize the relationship between RT and elevated temperature properties. These data and the RT reference properties are summarized in Table 4. Fiber Lot 8S-125 was selected for the initial CVD coating parametric study and Lots 8S-123A and 8S-124 were selected for scale-up production of HfC coated SiC filament.

Several lots of filament evaluated in the previous program (NAS3-18921) were given in vacuo thermal exposures of 200 hr at 982°C. The as-received RT and 982°C tensile data are compared to the thermally exposed RT and 982°C tensile strengths in Table 5. Fiber Lots 8S-69, 8S-80, and 8S-662 were CVD tungsten coated. There is an interesting comparison of properties of the uncoated vs W-coated fiber lots. Uncoated, unexposed materials display a characteristic decrease in tensile properties between RT and 982°C. A drastic decrease also occurs after the 200 hr thermal exposure. This must be due in part to interactions between the tunsten core and SiC, and possibly to surface damage during the thermal exposure handling. The small but significant increase in strength of the thermally exposed material at 982°C over that at RT was unexpected. A possible explanation is a decrease in notch sensitivity of W-core SiC filament at elevated temperatures.

TABLE 3

Room Temperature Tensile Properties of SiC Filament (25 mm gauge length)

Lot #	# Revs*	Diameter mm	Diameter in. x 10^3	σ** ksi	σ** MPa	σ_{max} ksi	σ_{max} MPa	σ_{min} ksi	σ_{min} MPa	Std Dev ksi	Std Dev MPa	Vendor ksi
8S-120	5040											440
8S-121	7230	143.0	5.63	441.2	3041	495.4	3413	362.7	2503	60.5	417	400
8S-122	4000	145.3	5.72	386.6	2668	442.4	3048	266.3	1834	57.2	374	440
8S-123A	3656	143.5	5.65	497.5	3434	514.5	3547	455.6	3144	19.7	136	480
8S-123B	675	144.8	5.7	495.0	3413	522.8	3606	354.3	2441	50.0	345	480
8S-124	1300	151.6	5.97	511.3	3523	540.2	3723	402.2	2772	40.8	281	500
8S-125	3912	147.8	5.82	541.4	3730	556.0	3834	526.9	3634	10.4	72	440
8S-126	1850	149.9	5.9	527.0	3634	564.6	3893	483.9	3337	24.8	171	510
8S-127	6634	146.8	5.78	496.1	3420	520.4	3585	444.9	3068	20.9	144	480
8S-132	5912	145.3	5.72	463.5	3200	494.0	3406	360.8	2489	49.6	342	480
8S-133	5878	144.3	5.68	448.1	3090	512.8	3537	365.1	2517	52.1	359	480
8S-134	14167	148.1	5.83	430.7	2971	478.5	3303	354.8	2448	53.8	371	480
8S-135	6277	144.8	5.70	482.6	3330	509.8	3516	371.6	2565	49.0	538	470
8S-138	6466	143.5	5.65	432.7	2990	496.9	3427	369.4	2544	57.0	393	440
8S-140	275	138.9	5.47	455.0	3137	526.1	3627	385.2	2655	60.0	414	437
8S-160	4444	143.0	5.63	456.0	3144	495.4	3413	424.6	2930	54.3	373	450
8S-161	967	142.7	5.62	464.5	3206	489.5	3379	391.6	2703	31.9	220	478
8S-162	2920	140.5	5.53	460.2	3172	484.9	3344	430.0	2965	16.7	115	440
8S-163	2126	144.3	5.68	373.8	2578	486.7	3358	260.8	1800	69.5	470	446
8S-164	5720	140.5	5.53	491.5	3389	513.5	3544	476.8	3289	11.6	80	440
8S-166	4682	143.5	5.65	467.9	3227	483.7	3337	448.5	3092	11.6	80	450
8S-167	10152	145.3	5.72	437.3	3013	455.3	3137	420.9	2903	11.7	81	405
8S-168	3257	142.2	5.60	446.7	3082	483.4	3330	402.3	2772	44.8	309	450
8S-169	2069	141.0	5.55	440.2	3034	455.7	3144	428.4	2951	11.4	79	420
8S-171	2086	142.7	5.62	464.5	3203	480.6	3316	453.9	3130	9.2	63	440
8S-117	1805	141.7	5.58	487.2	3368	522.3	3600	459.3	3164	21.6	149	450
8S-62	1825	141.1	5.555	429.3	2958	446.6	3082	410.2	2827	12.5	86	400

* Number of revolutions on an 8" dia spool, as received.

** Average of 10 tests.

TABLE 4

Room Temperature and 982°C Tensile Strengths of Selected Fiber Lots

	R.T. Tensile Strength				982°C (1800°F) Tensile Strength			
	$\bar{\sigma}$		Std. Dev.*		$\bar{\sigma}$		Std. Dev.*	
Lot No.	ksi	MPa	ksi	MPa	ksi	MPa	ksi	MPa
8S-117	487.2	3360	21.6	149	226.3	1560	29.9	206
8S-123A	497.5	3430	19.7	136	294.6	2030	38.7	267
8S-124	511.3	3520	40.8	281	319.8	2210	29.7	205
8S-125	541.4	3730	10.4	72	314.1	2170	39.5	272
8S-126	527.0	3630	24.8	171	319.4	2200	44.9	310
8S-127	496.1	3430	20.9	144	219.1	1510	56.9	392
8S-135	482.6	3330	49.0	338	218.6	1510	22.3	154
8S-163	373.8	2580	69.5	470	205.4	1420	33.9	334
8S-114	491.5	3390	11.6	80	300.2	2080	31.2	215
8S-166	467.9	3230	11.6	80	228.7	1580	24.5	169
8S-164	491.5	3389	11.6	80	--	--	--	---

* Results of 10 tests.

TABLE 5

Tensile Strength of Thermally Exposed SiC Filament - ksi (MPa)

Lot No.	$\bar{\sigma}$ (Mean)	$\sigma_{Maximum}$	$\sigma_{Minimum}$	Standard Deviation	As Received σ (mean)
RT Test After 200 hr Exposure at 982°C (1800°F)					
8S-100	217(1496)	242(1669)	197(1358)	13.9(95.8)	450(3103)
8S-69*	163(1124)	322(2220)	125(862)	54.1(373.0)	446(3075)
8S-662*	184(1269)	206(1420)	161(1110)	10.8(74.5)	434(2992)
8S-106	214(1476)	233(1607)	197(1358)	10.9(75.2)	460(3172)
8S-98	238(1641)	269(1855)	152(1048)	36.8(253.7)	490(3379)
8S-80*	193(1331)	206(1420)	170(1172)	10.9(75.2)	414(2855)
982°C (1800°F) Test After 200 hr Exposure at 982°C (1800°F)					
8S-100	203(1400)	287(1979)	143(986)	47.2(325.4)	205(1414)
8S-69*	253(1744)	269(1855)	241(1662)	9.5(65.5)	294(2027)
8S-662*	312(2151)	376(2593)	269(1855)	42.1(290.3)	296 (2068)
8S-106	287(1979)	340(2344)	170(1172)	50.4(347.5)	197(1358)
8S-98	278(1917)	340(2344)	224(1544)	49.3(339.9)	208(1434)
8S-80*	365(2517)	376(2593)	340(2344)	15.1(104.1)	343(2365)

* W coated

The CVD W-coated lots 8S-80 and 8S-662 were even more interesing in behavior in that the 982°C strength actually improved after a 200 hr thermal exposure at 982°C. Inversely, the RT strength of the W-coated lots was drastically lower after thermal exposure. These effects again must be related to a decreased notch sensitivity at 982°C as compared to ambient temperature, i.e., surface interaction of SiC and tungsten decreases fiber strength at RT. At 982°C the tungsten must actually contribute to the fiber strength.

Strength of HfC Coated SiC. The RT tensile strengths of developmental lots of HfC coated SiC filament are given in Table 6. A deterioration of strength is noted after coating. These filament strength data are plotted vs coating thickness in Fig. 36. The functional relationship appears to follow a Griffith-type form. This relationship may be explained by the structure of the coating. An SEM examination of the coated filament revealed a very tenacious HfC coating that resisted spalling. The SEM photograph in Fig. 37 is of a specimen taken from a tensile test where a severe shock accompanies the rupture. The columnar structure of the coating noted in this photograph and the brittle nature of HfC must be related to the Griffith-type behavior of coated filament.

The dark layer at the interface between the coating and the SiC substrate was examined by energy dispersion X-ray analysis and did not appear to be related to interdiffusion of SiC and HfC. The scattering efficiency of electrons is proportional to the atomic number of the target. A layer darker in appearance should be composed of a substance with a lower average atomic number than SiC. We assume that the layer is supersaturated with carbon. This layer is either formed during filament processing or it forms during decomposition of methane during the initial coating operation. The dark layer is also visible in the optical micrographs in Fig. 38 and in the post-HIP condition in Fig. 39. The optical photomicrographs of the filament after HIP, 2 hr at 1025°C (1875°F), 207 MPa (30 ksi), show the structure of the coating and the dark layer to be unaltered by thermal exposure.

TABLE 6

Room Temperature Tensile Strength of CVD HfC Coated SiC(W) Filament

Lot		Coating Thickness μm	σ_{ave}* ksi	σ_{ave}* MPa	σ_{max} ksi	σ_{max} MPa	σ_{min} ksi	σ_{min} MPa	Standard Deviation ksi	Standard Deviation MPa
8S-73	Single pass		325	2241	405	2793	221	1524	59.6	392
"	Double pass		269	1855	313	2158	188	1296	33.8	233
8S-125	Uncoated (5.82 mil dia)		541	3730	556	3830	527	3630	10.4	72
Run #22	Single pass	6.5	270	1862	295	2034	224	1544	20.4	141
23		6.5	270	1862	295	2034	224	1544	21.0	145
24	"	6.5	257	1772	287	1979	233	1606	20.3	140
26	"	6.5	237	1634	278	1917	206	1420	25.3	174
27	"	6.5	216	1800	278	1917	251	1731	14.9	103
29	"	8.5	199	1374	209	1441	185	1269	9.1	63
30	"	9.0	223	1538	232	1600	191	1317	12.5	86
31	"	7.4	229	1579	243	1674	203	1400	12.6	87
31	(end)**	7.4	221	1524	238	1641	200	1379	11.6	80
35	(end)	5.9	264	1820	302	2085	259	1785	19.4	134
36	(end)	6.1	273	1882	296	2043	249	1722	16.7	115
36	(beginning)		295	2034	312	2151	282	1944	10.2	70
37	(beginning)	5.3	288	1987	306	2110	241	1660	30.3	209
38	(end)	5.2	291	2006	313	2160	263	1814	12.5	86
38	(beginning)		300	2068	371	2555	253	1747	37.0	255
39	(beginning)	4.0	369	2541	403	2777	346	2388	17.5	121
39	(middle)		374	2579	410	2826	328	2259	24.5	167
39	(end)		358	2470	530	3654	248	1710	97.7	674

* Average to 10 tests.

** Position of sample with respect to coating sequence.

X-ray diffraction analyses were conducted on the coated filament from several lots of material. The results and atomic percent carbon inferred from the lattice parameter data are tabulated below.

8S-125 Run	Lattice Parameter Å	Atomic % Carbon
35	4.6483	53.0
36	4.6495	53.6
37	4.6475	52.5
38	4.6490	53.4
39	4.6477	52.8

These data indicate that the HfC coatings are also supersaturated with carbon.

We conclude this section by stating that a number of things happen to the filament, all of which to some degree deteriorate the tensile strength. The deterioration processes are associated with the following:

1) Interaction between filament and the tungsten core after extended thermal exposure.
2) Griffith relationship between coating thickness and strength of filament.
3) Coating defects resulting in interaction between matrix and filament.
4) Columnar structure of the HfC barrier coating.

Further research on the HfC coating is necessary. Specifically, the effect of stoichiometry and coating morphology should be further evaluated.

5. COMPOSITE CHARACTERIZATION

The strength values obtained have been inadequate.+ 982°C (1800°F) strengths have been just a few thousand psi greater than unreinforced matrix values and RT values have been 40% less than the base line matrix strength.

Composite Tensile Tests. The first composites evaluated were tungsten coated lots of material. Tensile specimens were EDM machined from panel 8S80-5. The strengths are tabulated below.

Specimen*	RT UTS - ksi (MPa)
8S80-5A	37.2 (256)
8S80-5B	58.8 (405)
	982°C (1800°F UTS - ksi (MPa)
8S80-5-1	12.45 (85.84)
8S80-5-2	11.82 (81.50)

* 25 mm gage length for RT test, 15.2 cm long strip with 20 mm heated zone for 982°C (1800°F test.

Radiographs of the room temperature specimens are shown in Fig. 40. The location of the fractures correspond with a warpage or misalignment of the filament in specimen A and a local matrix thinning in specimen B. The metallographic data of this particular composite panel was discussed earlier in reference to Fig. 27 and 28. A number of defects were noted at that time which apparently contributed to the low strengths.

High hopes were held for the first experimental lot of HfC coated filament. These filaments were composited into panels P154.

+ See note at the end of this section.

The following strengths were measured:

Test No.	Test Temperature °C	Test Temperature °F	UTS MPa	UTS ksi	Waspaloy UTS ksi
P154-1(50 v/o)	760	1400	417	60.4	115
P154-2(50 v/o)	982	1800	147.5	21.4	18.9

Again the values were significantly lower than rule-of-mixture predictions. A SEM examination of the fracture surfaces in Fig. 41 shows the L/D ratio of pulled out filament to be approximately 12. The shearing took place at the interface between the coating and the filament, as shown in Fig. 41. This phenomenon occurred at both 982°C and 76°C.

The last panel investigated was P40-38(nominal 50 v/o within the composite bundle) and was made from production HfC coated filament. The RT and 982°C (1800°F) strength is given below.

Test No.	Test Temperature °C	Test Temperature °F	UTS MPa	UTS ksi	Modulus X 10^6 psi	Modulus MPa
P40-38-1A	RT	RT	574	82.2	37.8	2.61 x 10^{11}
P40-38-2A	RT	RT	557	79.7	37.0	2.55 x 10^{11}
P40-38-2	982	1800	147	21.0	--	---
P40-38-3	982	1800	107	15.3	--	---

Modulus values were approximately 5 x 10^6 psi less than rule-of-mixture of a 39 v/o composite (including a 50 v/o fiber bundle and extra matrix cladding used for surface protection).

The low temperature strength of this panel, though still inadequate, was an improvement over that of the tungsten barrier coated material discussed earlier. The high temperature strength was little changed.

There is greater evidence of the tenaciousness of the coating in Fig. 42. Although most pulled-out filaments were stripped of the barrier coating, numerous examples of adherent HfC were noted. This adherence was also noted in the room temperature tested specimens.

NOTE: Work performed on NSF Grant #DMR-76-0286 has a direct bearing on the results presented here. A composite was fabricated having ∿15 v/o HfC coated SiC filament reinforcement. This panel was tested at RT and 982°C (1800°F). The following results were obtained.

Specimen No.	Test Temperature °C	°F	UTS ksi	MPa
P57-39-3A	RT	RT	95.5	658
-3B	"	"	120.3	829
-1	982	1800	27.7	191
-2	982	1800	17.2	119

These values are considerably greater than those reported in this report for material containing twice the volume fraction of filament. Physical separation of the filament must be an important consideration. Calculations utilizing the actual volume fraction of the overall section revealed a filament stress of 586 MPa (∿85 ksi) from 191 MPa (27.7 ksi) 982°C data point. Although this is a significant improvement over previous results, the full strength potential of the filament has yet to be realized.

6. DISCUSSION

The strengths obtained from the panels were unsatisfactory. The reasons appear to be due to a combination of process related defects. The filament itself loses over half its strength as a consequence of the coating. If the barrier is imperfect chemical interaction takes place, further weakening the reinforcement. Finally, local movement of the matrix due to lateral extrusion during HIP or bubble formation and "mud cracking" during binder removal seem to finish the list of defects leading to loss of strength.

It is unfortunate that most of the effort on this program had to be directed toward compatibility considerations and barrier development. The defects discussed above, though requiring effort, can be eliminated. Work in progress under NSF grant on lower volume fraction composites has shed more light on the fabricating problems and lead us to be more optimistic as to the potential of SiC reinforced superalloys. In spite of the low strength results shown here, SiC reinforced superalloys with useful properties are within reach and should be further investigated.

7. REFERENCES

1. Cornie, J. A.,"A Kinetic and Microstructural Study of Oxide, Carbide, and Nitride Diffusion Barriers in HSTW (Tungsten) Reinforced Superalloy Composites". To be published ICCM-II, April 1978, Toronto.
2. Cornie, J. A., Cook, C. S., and Andersson, C. A., Fabrication Process Development of SiC/Superalloy Composite Sheet for Exhaust System Components, NASA-CR-134958, January 1976.
3. Petrasek, D. W. and Weeton, J. W., "Alloying Effects on Tungsten-Fiber-Reinforced Copper Alloys on High-Temperature Alloy Matrix Composites", NASA TND-1568, October 1963.
4. Grünling, H. and Hofer, G., "Verzögerung der Rekristallisation von Wolframdraht in Ni und NiCr Matrix", Z. F. Werks Hofftechnik, J. of Materials Technology, 5, pp 9-72, January 1974.
5. Petrasek, D. W. and Signorelli, R. A., "Stress Rupture Strength and Microstructural Stability of Tungsten-Hafnium-Carbon Wire Reinforced Superalloy Composites", NASA TND-7773.
6. Mazzei, P., Private Communication.

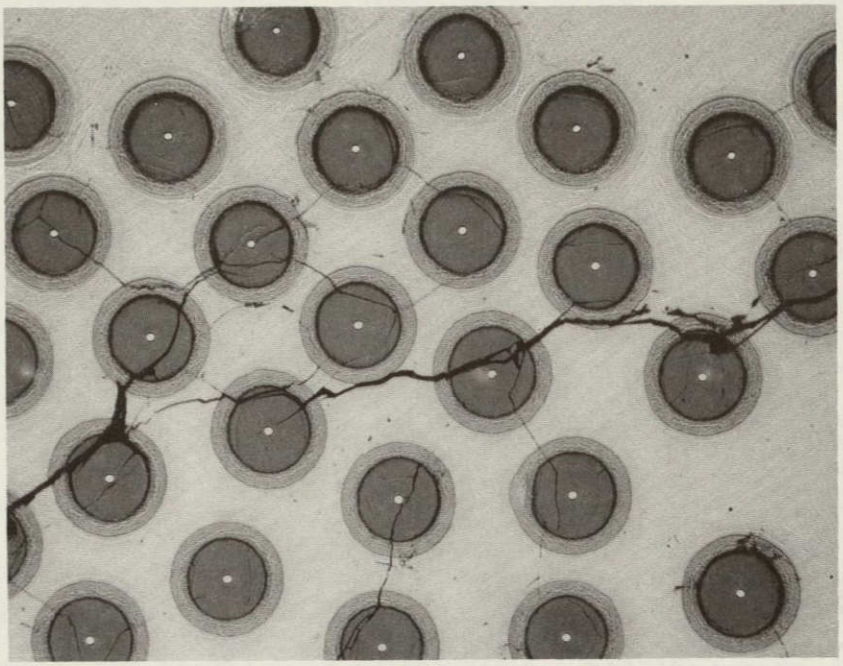

A) 100 X

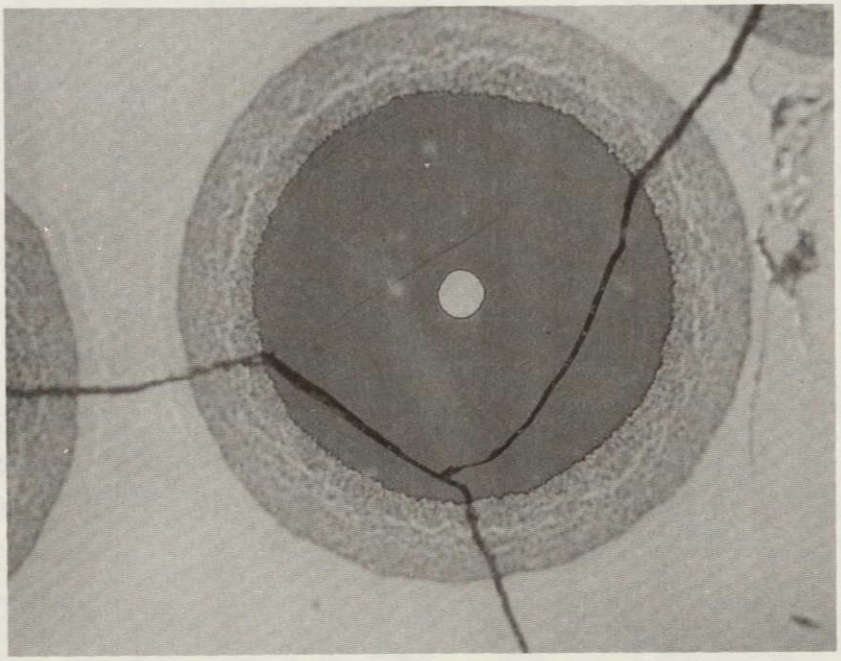

B) 500 X

N-2437

Fig. 1. Microstructure of SiC/Hastelloy X Composite After HIP, 2 Hours at 1825°F (996°C), 15,000 psi

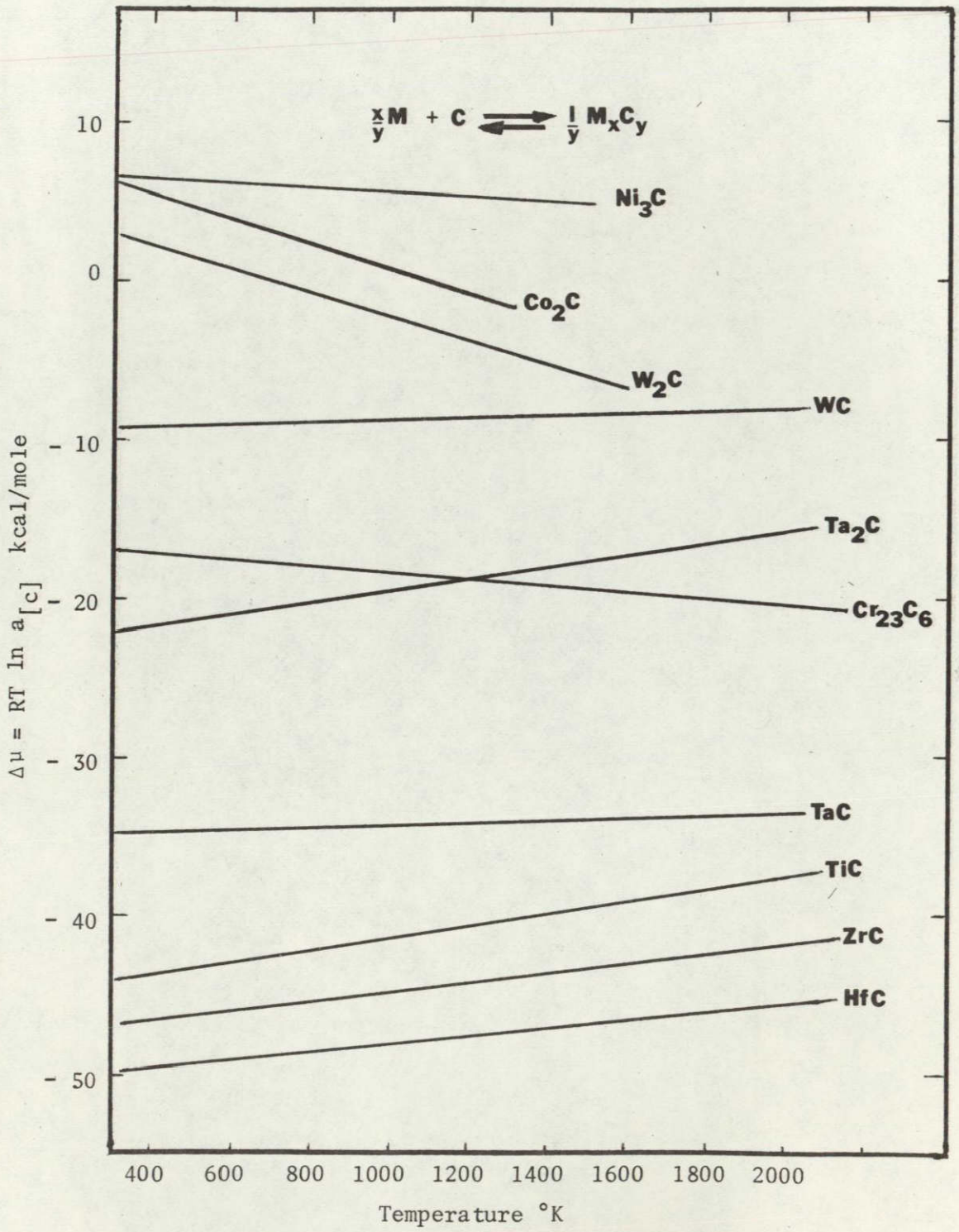

Fig. 2 -- Chemical potential of carbon for selected carbides

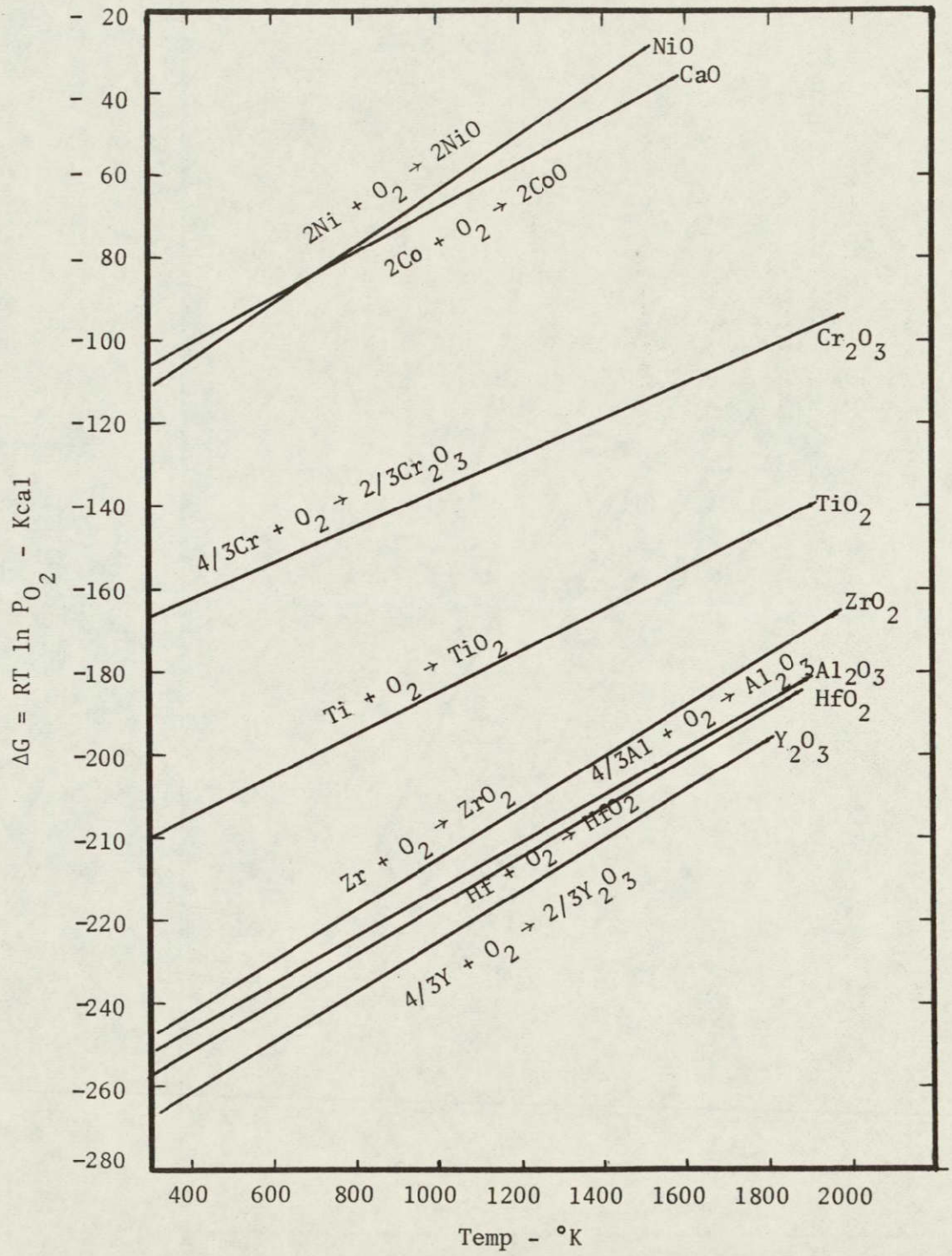

Fig. 3 -- Standard free energy of formation of selected oxides for the reaction $2\ x/y\ M + O_2 \rightleftarrows 2/y\ M_xO_y$

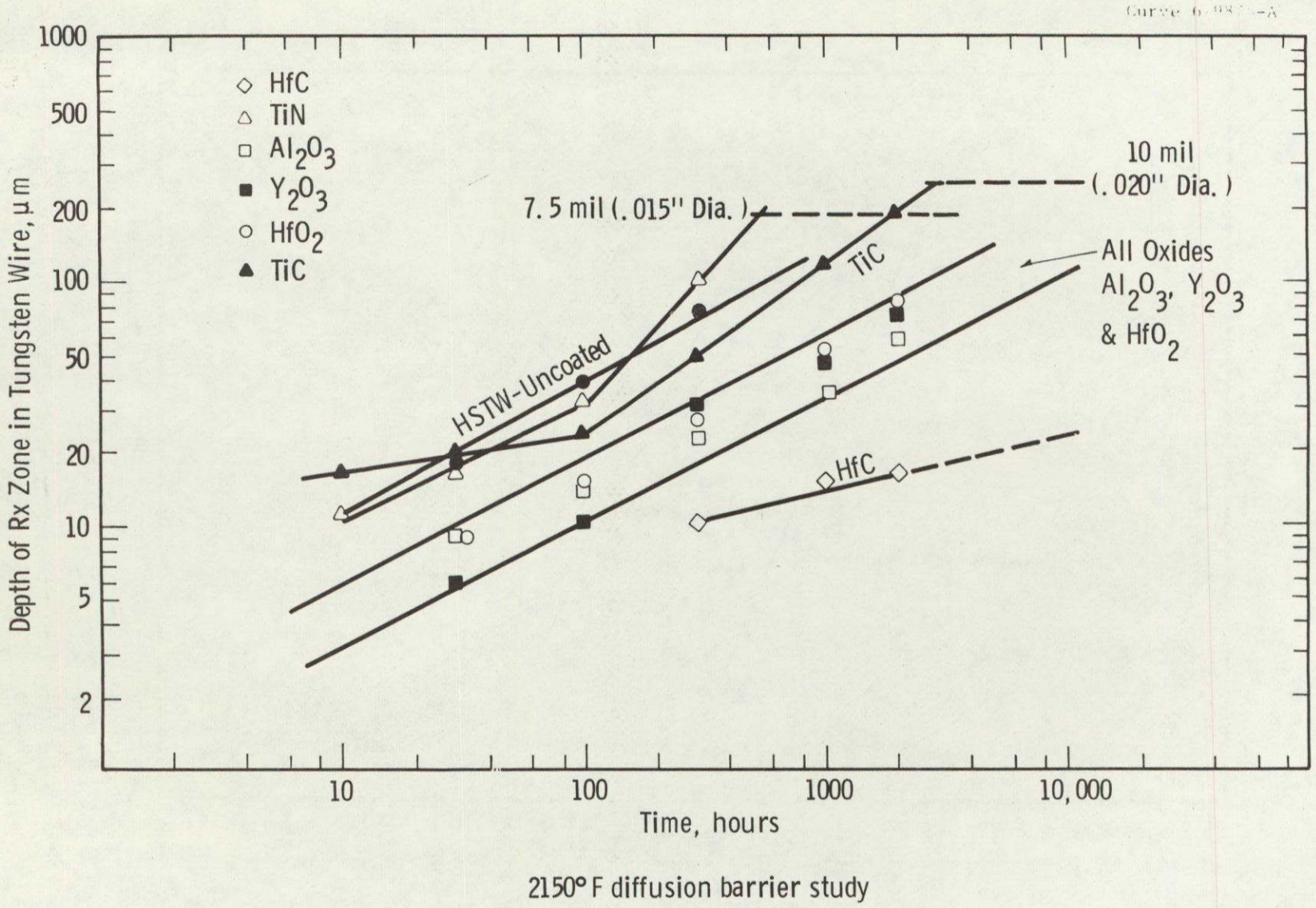

Fig. 4. Kinetic Data From 2150°F Diffusion Barrier Study

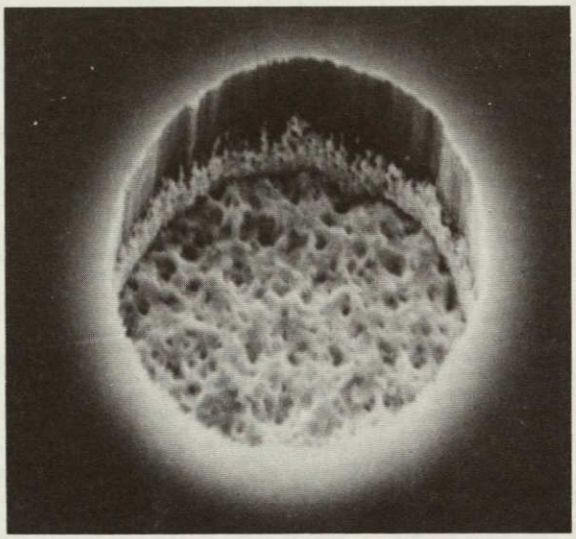

4000 X

4 hr. at 1800°F

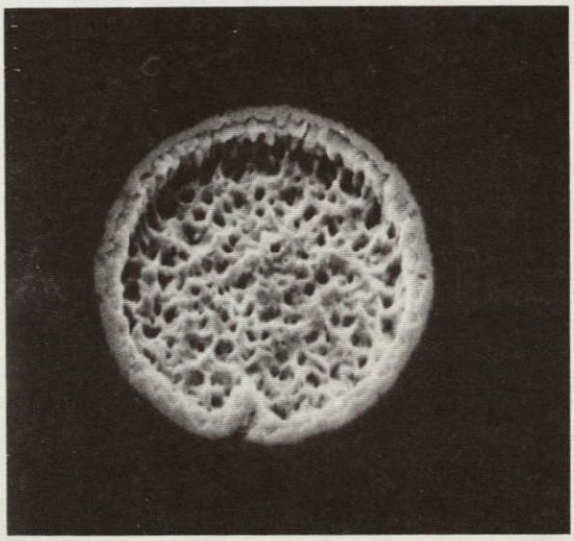

4000 X

200 hr. at 1800°F

Fig. 5. Growth of Intermediate Phases Between Tungsten Core and SiC at 1800°F.

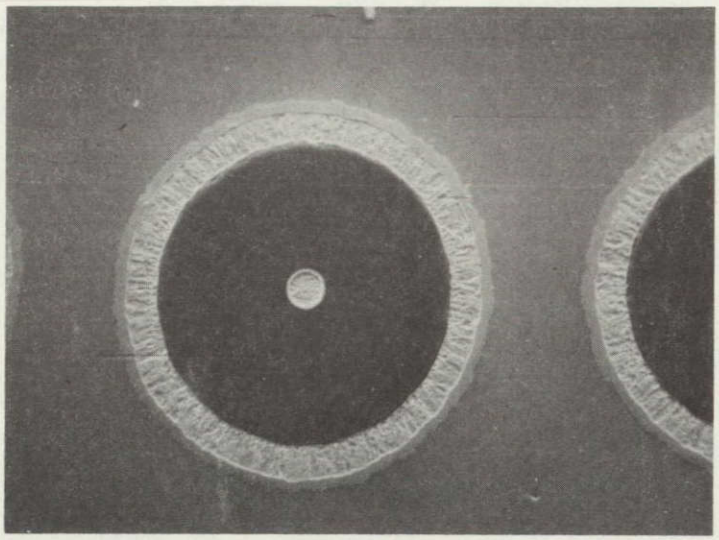

400 X

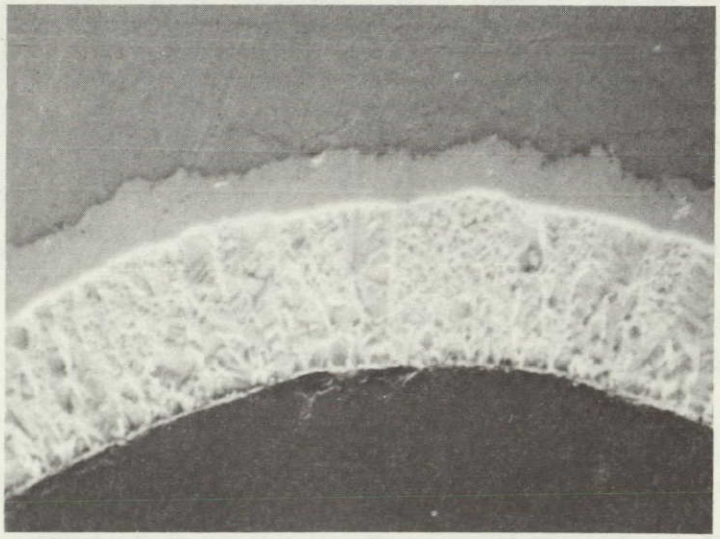

2000 X

Fig. 6. Chemical Interaction Between Waspaloy and CVD W Coated SiC After 200 Hours at 982°C (1800°F).

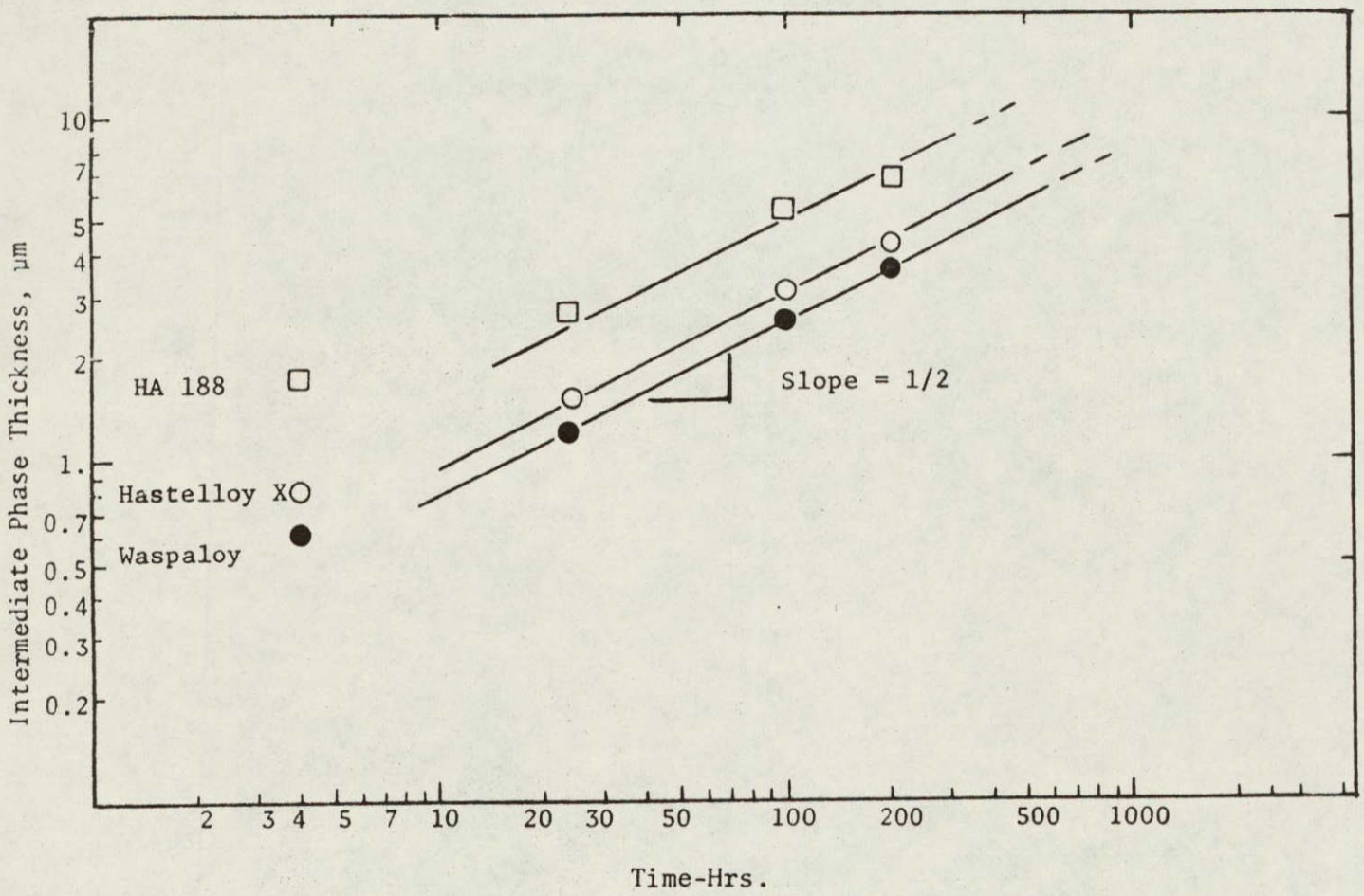

Fig. 7. Growth Kinetics of Intermediate Phase Between Candidate Matrix Alloys and CVD Tungsten Coated SiC at 982°C (1800°F)

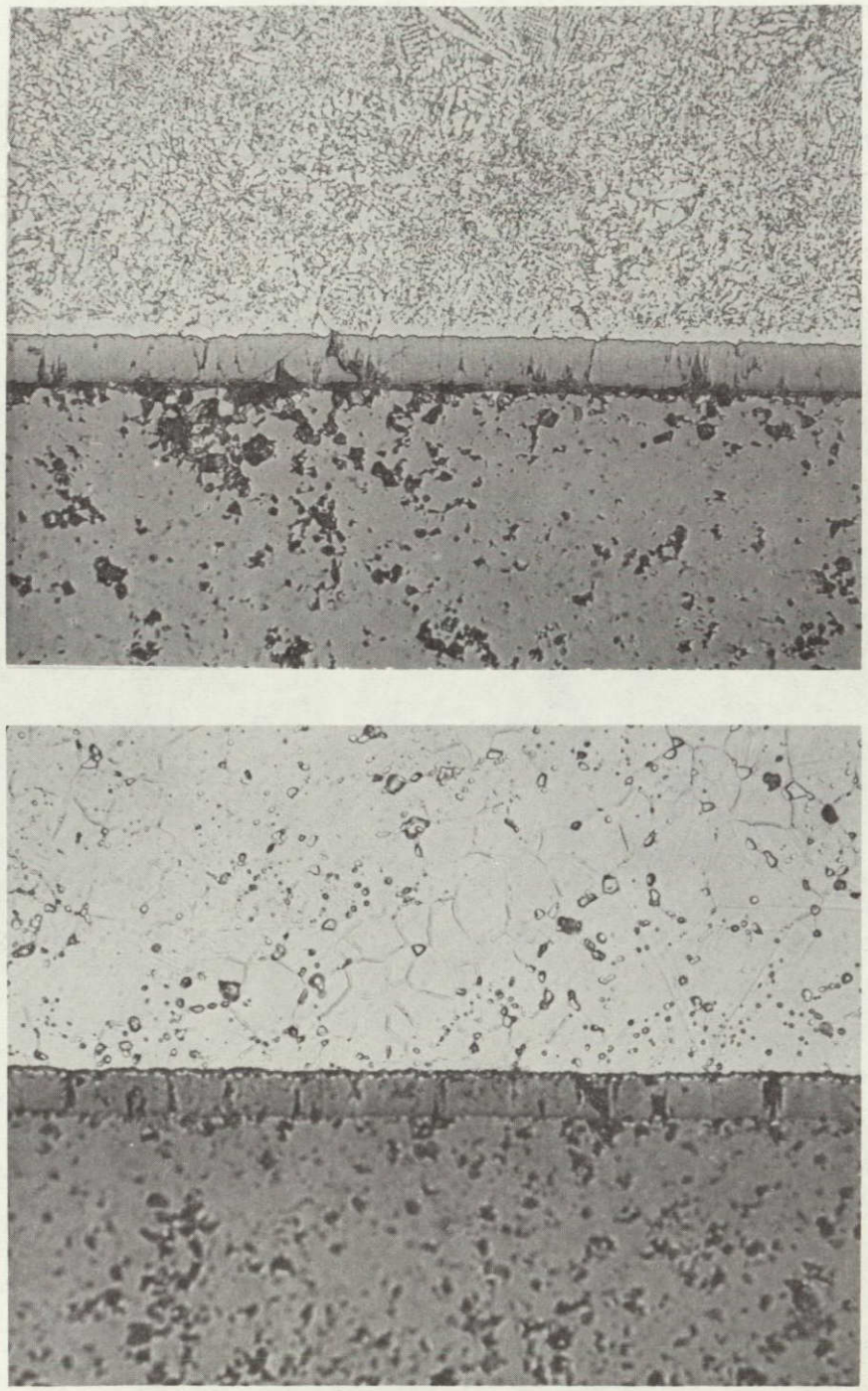

Fig. 8. Diffusion Couples Between Waspaloy and RF Sputtered HfC on a SiC Substrate, as HIP (a) and After 200 Hours at 982°C (1800°F (b).

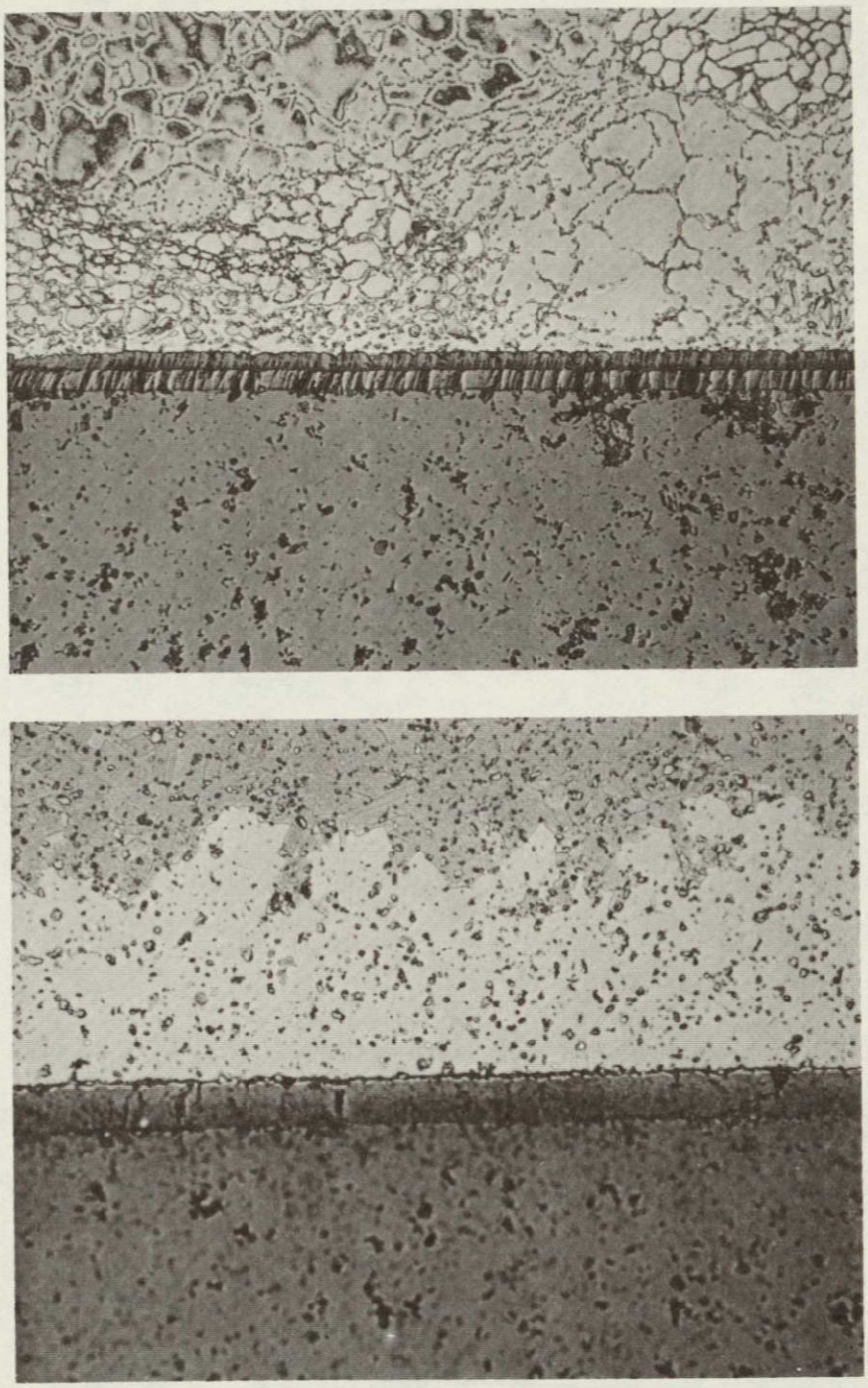

Fig. 9. Diffusion couple between HA-188 and RF sputtered HfC on a SiC substrate, as HIP consolidated (a) (996°C (1825°F), 138 MPA (20 ksi), 2 hr) and after 200 hrs at 982°C (1800°F) (b).

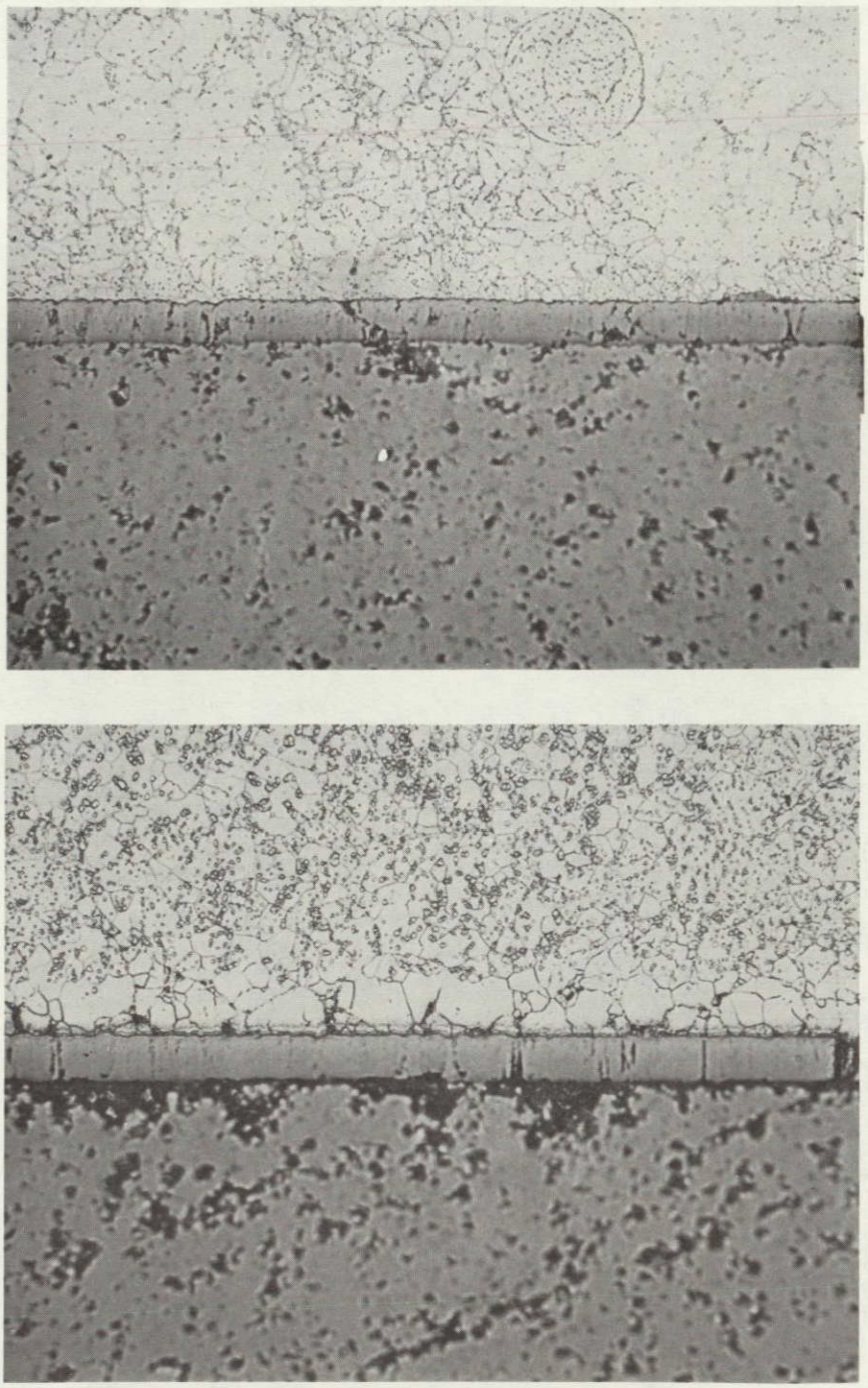

Fig. 10. - Diffusion couple between Hastelloy X and RF sputtered HfC on SiC substrate, as HIP (a) and after 200 hrs at 982°C (1800°F) (b).

As HIP
2 hrs @
996°C
(1875°F)

138 MPA
(70 ksi)

(a)

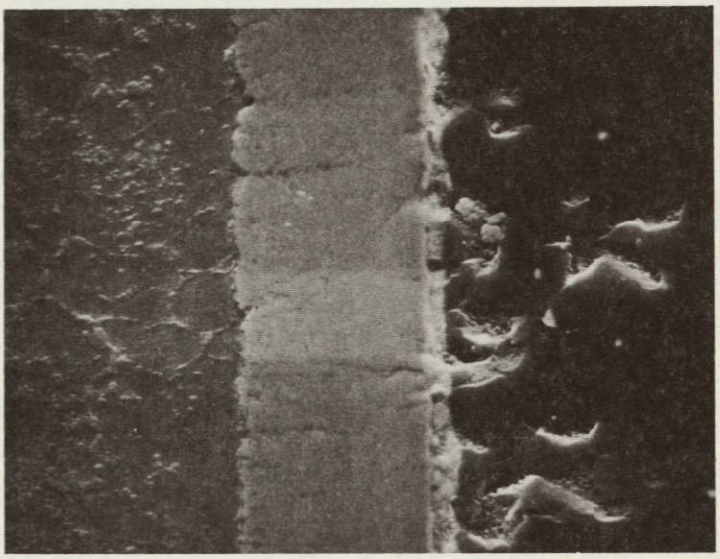

P-146
300X

200 hrs
@982°C
(1800°F)

(b)

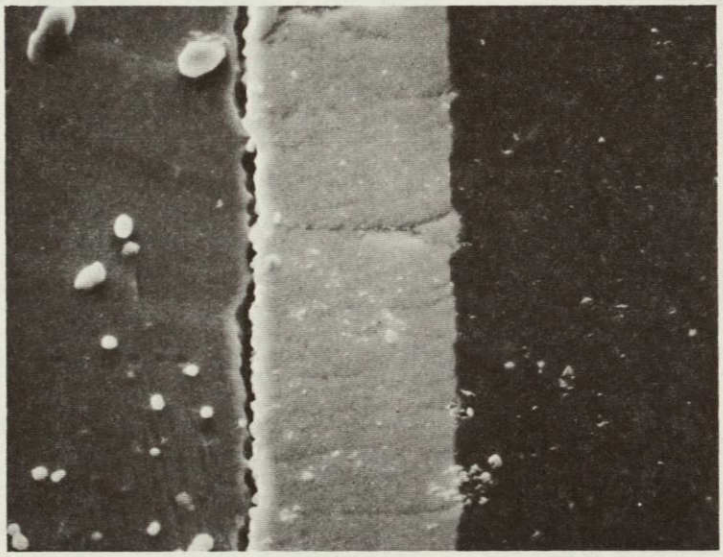

P-152
2500X

Fig. 11. SEM* of diffusion couple between Waspaloy (left), RF sputtered HfC (center) on a SiC substrate (right), as HIP (a) and after 200 hrs at 982°C (1800°F) (b).

*10% chromic-electrolytic etch

As HIP

(a)

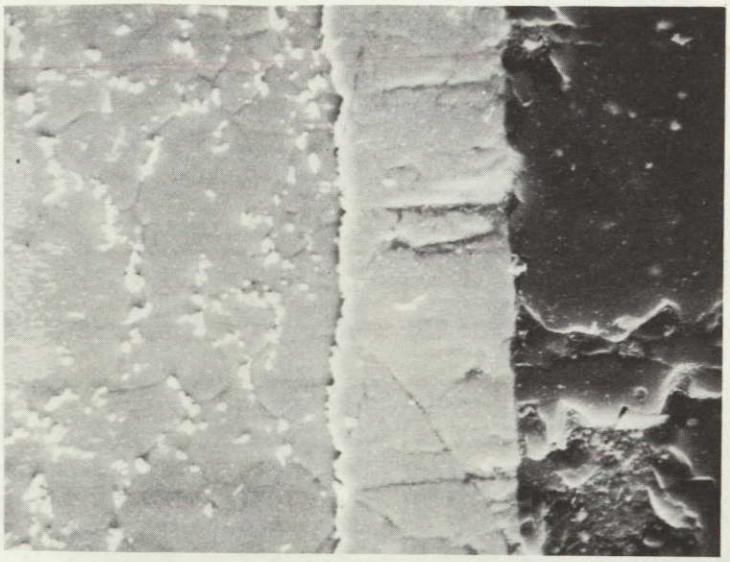

P-147
2300X

200 hrs
@982°C
(1800°F)

(b)

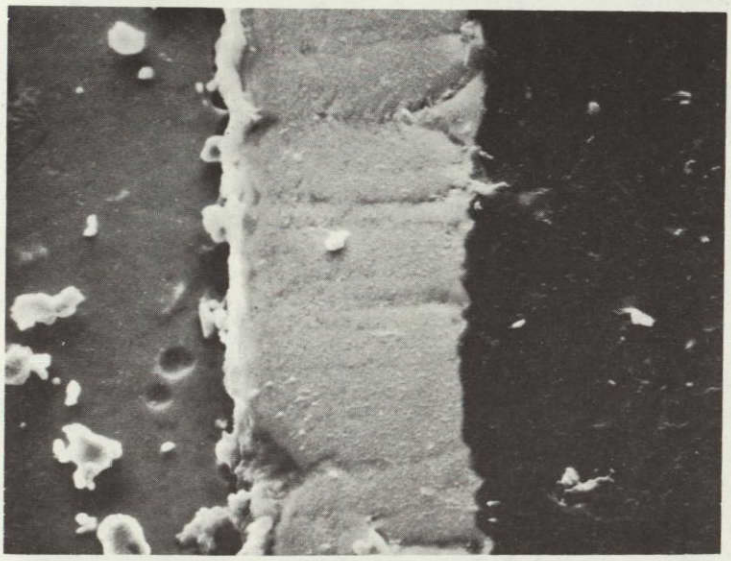

P-153
2500X

Fig. 12. SEM* of Diffusion Couple Between HA-188 (left) and RF Sputtered HfC (center) on a SiC Substrate (right), as HIP (a) and After 200 Hours at 982°C (1800°F) (b).

* 10% Chromic-electrolytic Etch

As HIP

(a)

P-148
2300X

200 hrs
@982°C
(1800°F)

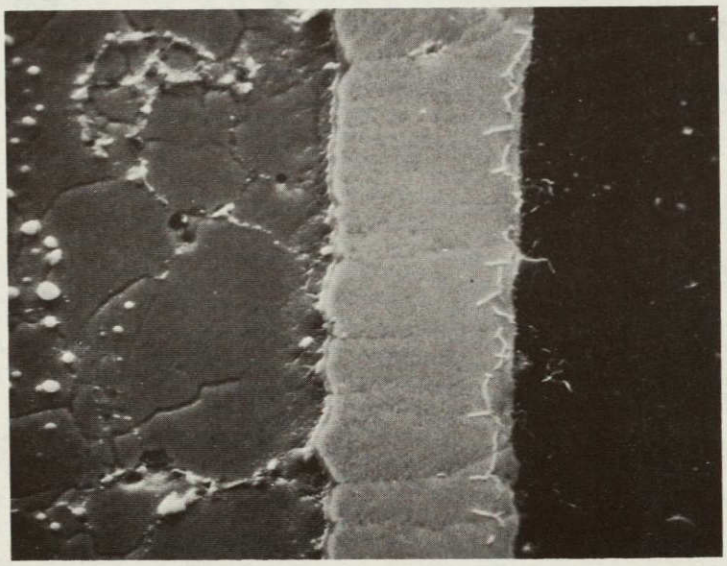

(b)

P-154
2300X

Fig. 13. SEM* of Diffusion Couple Between Hastelloy X (left) and RF Sputtered HfC (center) on a SiC Substrate (right), as HIP (a) and After 200 Hours at 982°C (1800°F) (b).

* 10% Chromic-electrolytic Etch

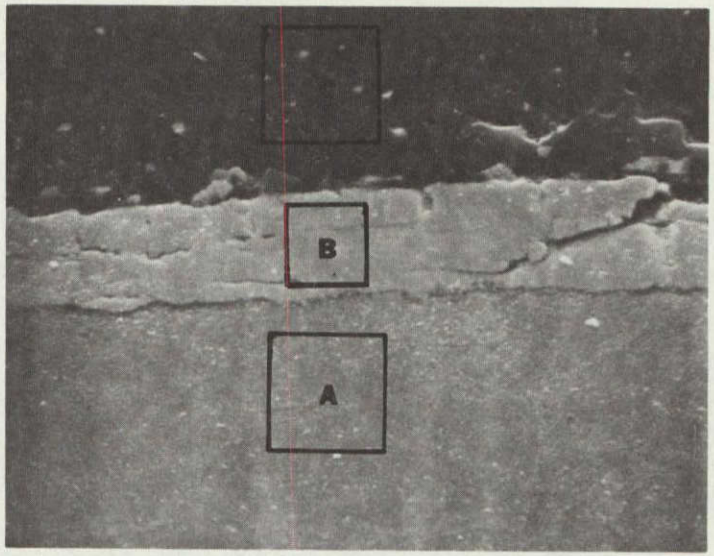

2000 X P-305

Areas Analyzed	Element-Radiation-keV-	Al Kα,β 1.49	Si Kα,β 1.74	Hf Mα 1.64	Hf Lβ 9.02	Mo Lα,β 2.29	Ti Kα 4.51	Cr Kα 5.41	Fe Kα 6.40	Co Kα 6.92	Ni Kα 7.41
A (Matrix)		408	--	--	--	1188	1082	6283	205	2548	9464
B (Barrier)		--	--	9292	1105	--	38	149	28	164	--
C (SiC)		--	10909	--	205	--	--	56	--	18	--

Fig. 14a. Waspaloy/HfC/SiC Diffusion Couple After 10 Hours at 1093°C (2000°F).

Microstructural and EDX Analysis of Selected Area

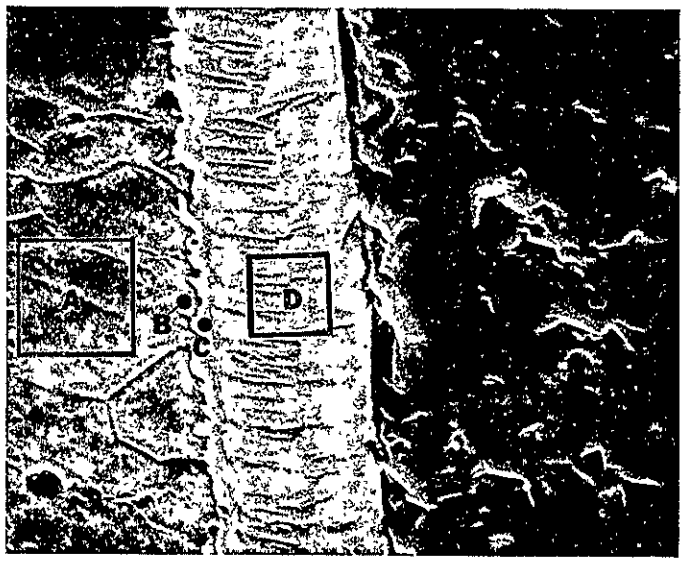

2000X P-302

Area Analysis	Element-Radiation-keV-	Al Kα,β 1.49	Si Kα,β 1.74	Hf Mα 1.64	Hf Lβ 9.02	Mo Lα,β 2.29	Ti Kα 4.51	Ca Kα 5.41	Fe Kα 6.40	Co Kα 6.92	Ni Kα 7.41	Zr 2.12
Area A (Matrix)		472	--	--	--	1176	552	7003	869	2724	9722	--
Spot B		681	--	--	--	1187	928	6954	757	2738	9773	--
Spot C		5392	1321	--	--	1834	9441	2561	170	924	3305	--
Area D		--	--	10,100	949	--	246	170	51	149	130	725

Fig. 15a. Waspaloy/HfC/SiC Diffusion Couple After 200 Hours at 1093°C (2000°F). Microstructure and EDX Analysis of Selected Areas.

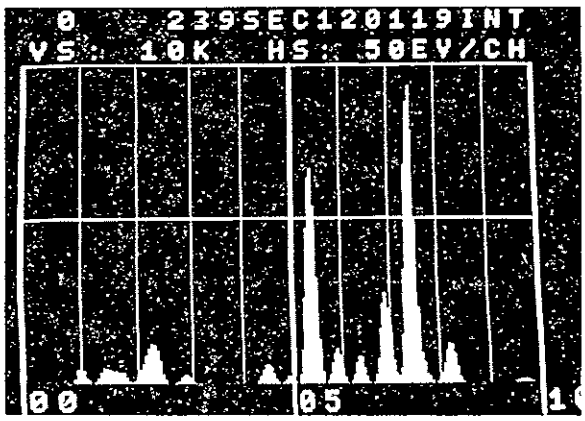

Area A Matrix

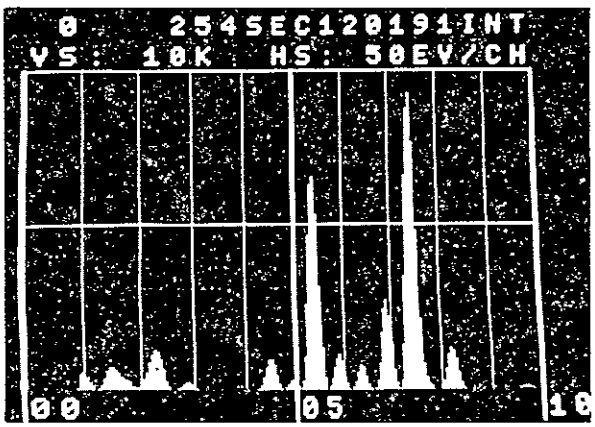

Spot B

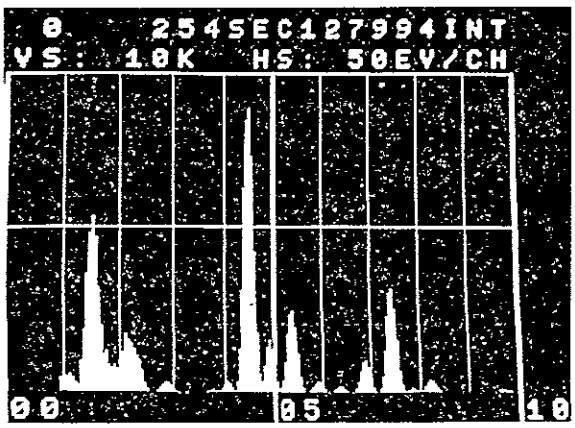

Spot C

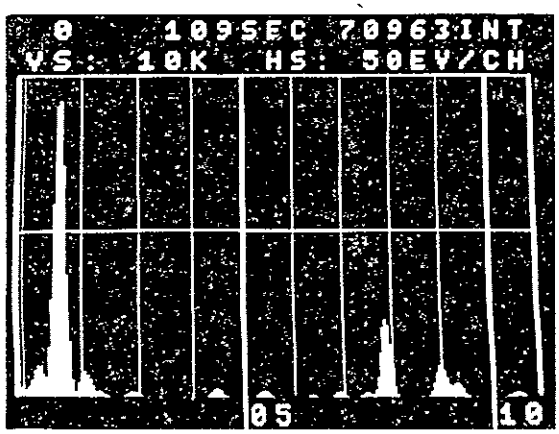

Area D

Fig. 15b. EDX Analysis of Selected Areas of Waspaloy/HfC/SiC Diffusion Couple After 200 Hours at 1093°C (2000°F).

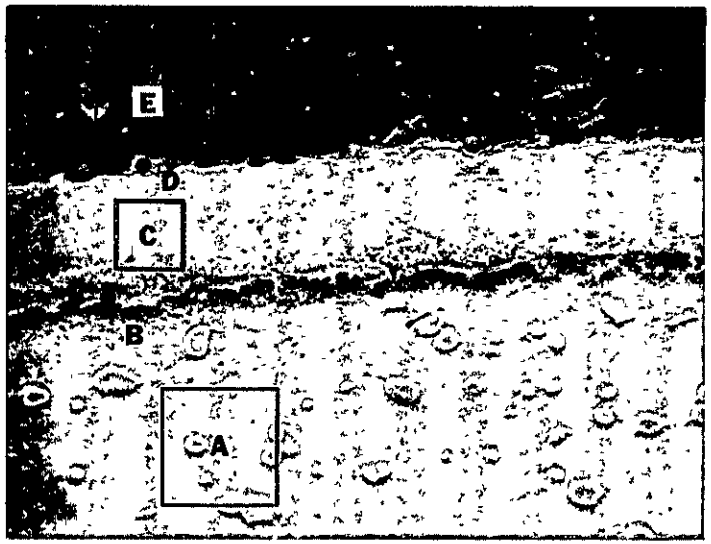

1200X P 304

Area	Element-Radiation-keV- Al Kα,β 1.49	Si Kα,β 1.74	Hf Mα 1.64	Hf Lβ 9.02	Mo Lα,β 2.29+	Cr Kα 5.41	Fe Kα 6.40	Co Kα 6.92	Ni Kα 7.41
Area A (Matrix)	231	525	--	--	2738	8175	5746	--	8940
Spot B	--	--	--	--	9.41	4101	1563	248	2588
Area C	--	--	9153	3425	--	309	116	133	--
Spot D	723	7634	--	--	--	9562	97	--	87
Area E	349	11,413	--	--	--	--	--	--	--

Fig. 16a. Hastelloy X/HfC/SiC Diffusion Couple After 200 Hours at 1093°C (2000°F). Microstructure and EDX Analysis of Selected Areas.

P- 304

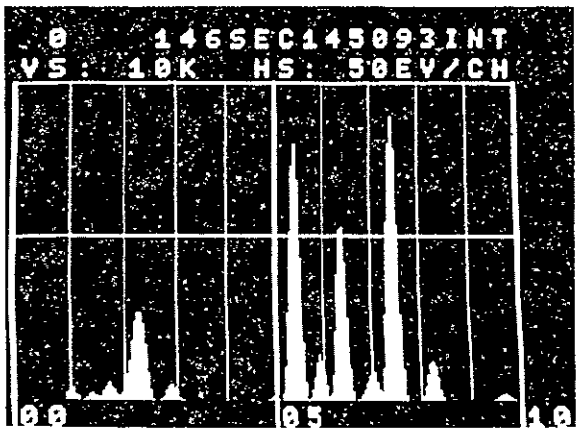

Area A

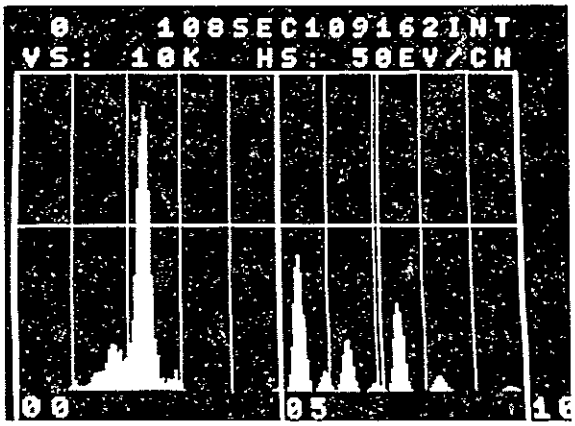

Spot B

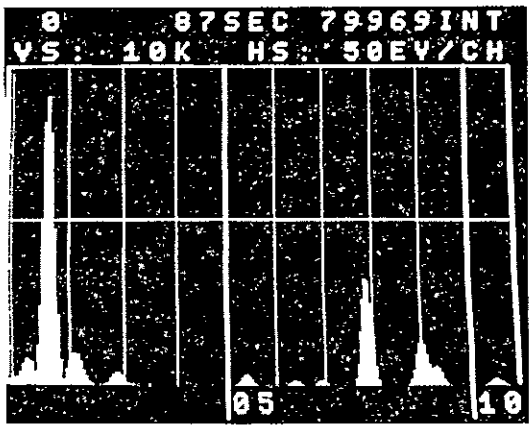

Area C

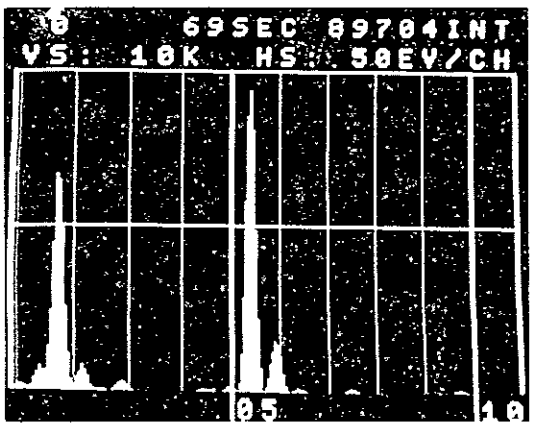

Spot D

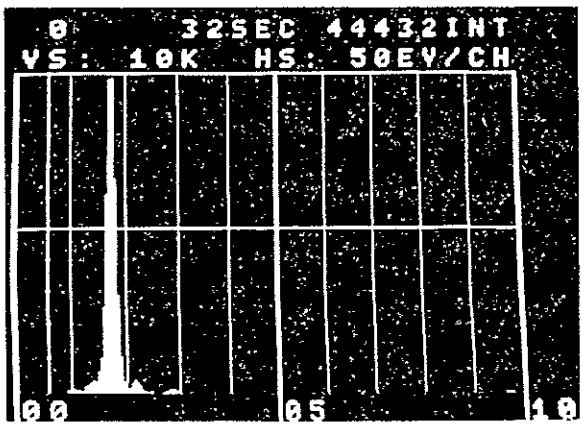

Area E

Fig. 16b. EDX Analysis of Selected Areas of Hastelloy X/HfC/SiC Diffusion Couple After 200 Hours at 1093°C (2000°F).

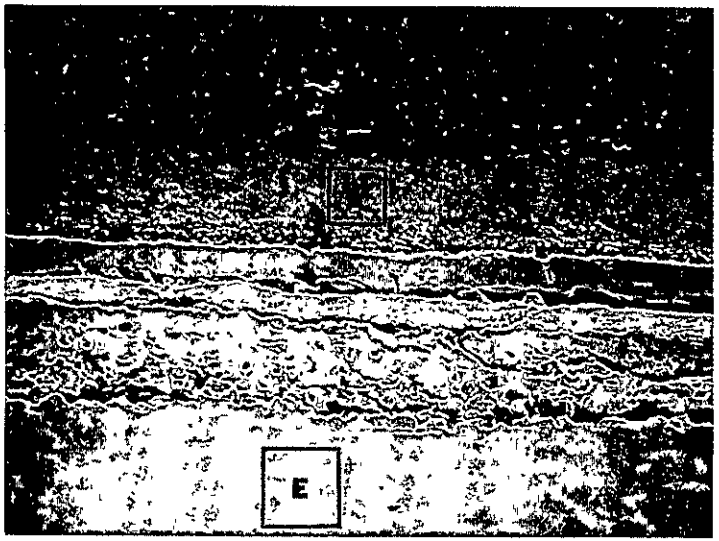

400X

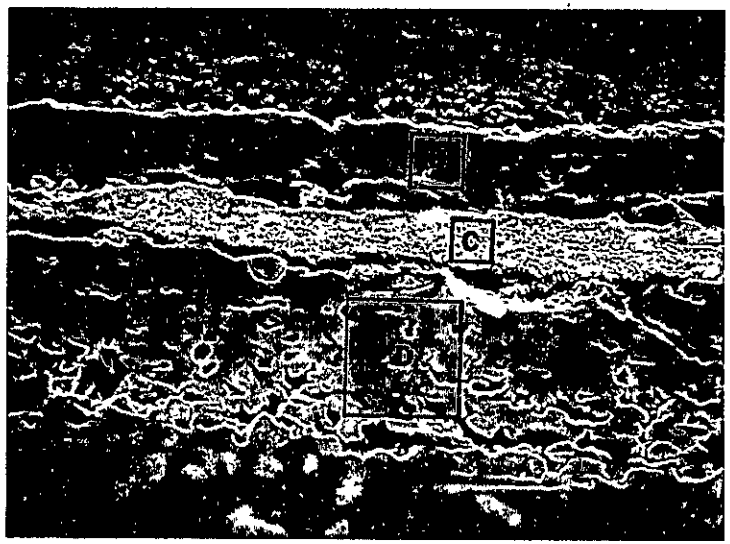

800X

P-303

Area Analyzed	Element-Radiation-keV-	Al Kα,β 1.49	Si Kα,β 1.74	Hf Mα 1.64	Hf Lα 7.90	Cr Kα 5.41	Mn Kα 5.89	Fe Kα 6.40	Co Kα 6.92	Ni Kα 7.47	W Lα 8.4	W Mα 1.77
Area A		--	8675	--	--	5349	--	107	4247	4925	631	*
Area B		--	5752	--	--	9137	--	59	1851	630	78	
Area C		--	--	9307	2255	283	--	51	225	--	--	--
Area D		781				9087	--	28	2630	1931	816	6938
Area E (Matrix)		801	*	--	--	7073	**	313	9202	3942	1017	6837

* Si Kα,β covered by Wm_{α}. ** Mn covered by CrKβ.

Fig. 17a. HA-188/HfC/SiC diffusion couple after 200 hr at 1093°C (2000°F). Micr structural and EDX analysis of selected areas.

P-303

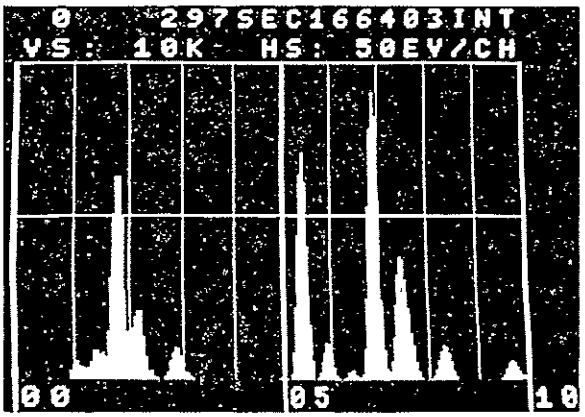

Area E - Matrix

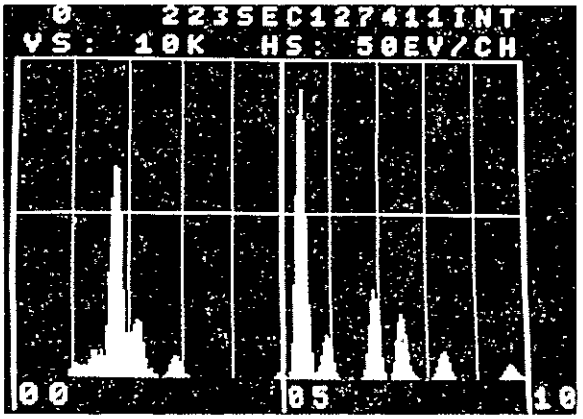

Area D

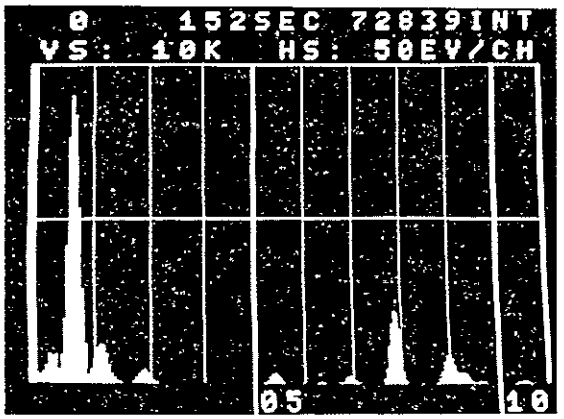

Area C

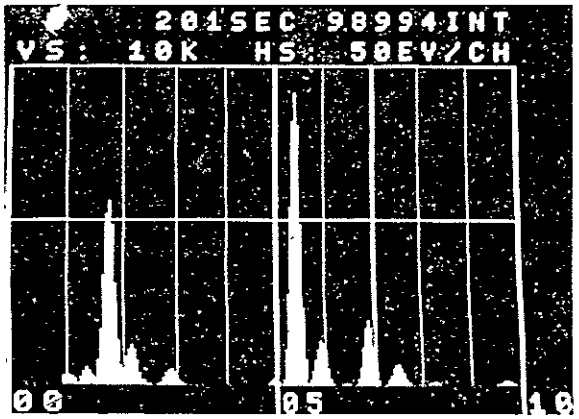

Area B

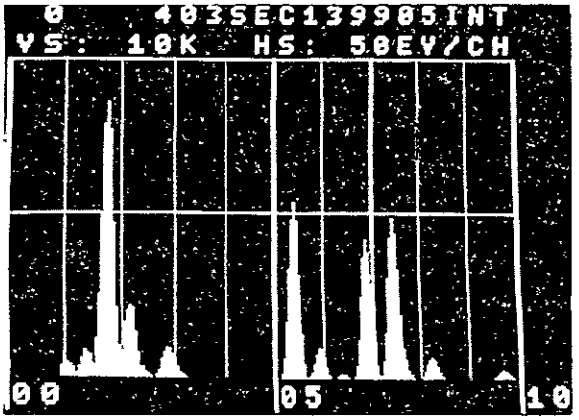

Area A

Fig. 17b. EDX analysis of selected areas of HA-188/HfC/SiC diffusion couple after 200 h at 1093°C (2000°F).

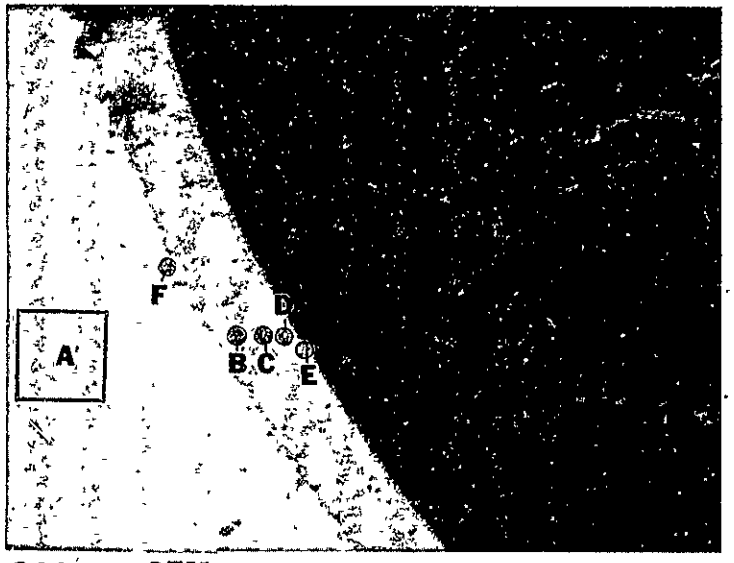

2600 X-SEM

1000 X- OM

	Counts Above Background					
Elem/Area	A	B	C	D	E	F
Si kα	200	25	270	295	3860	150
Mo 1αβ	750	--	--	--	--	290
Ti kα	208	3920	3890	3860	3050	3770
Cr kα	3600	--	--	--	10	1100
Fe kα	2290	--	30	39	--	750
Co kα	260	--	220	85	110	--
Ni kα	3740	--	--	--	--	1165

Fig. 18. Energy Dispersive X-ray Analysis of Interface Between TiN Coated SiC Fibers and Hastelloy X Matrix After 2 Hours HIP at 996°C (1825°F), 103 MPa (15,000 psi).

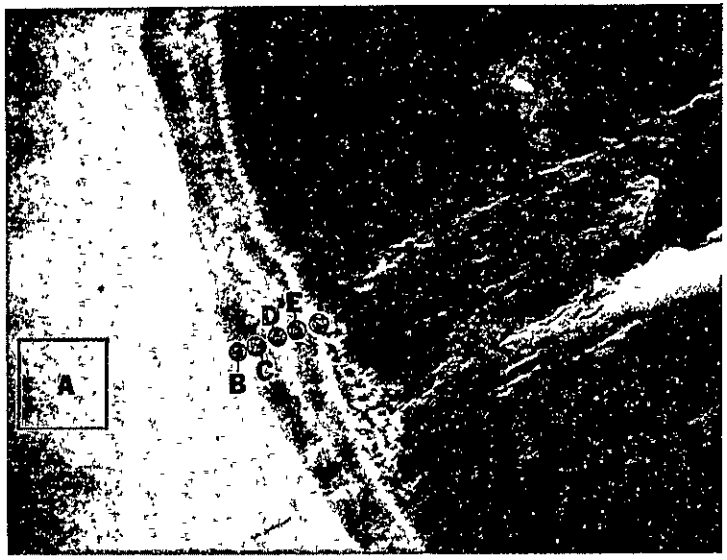

2700X -SEM

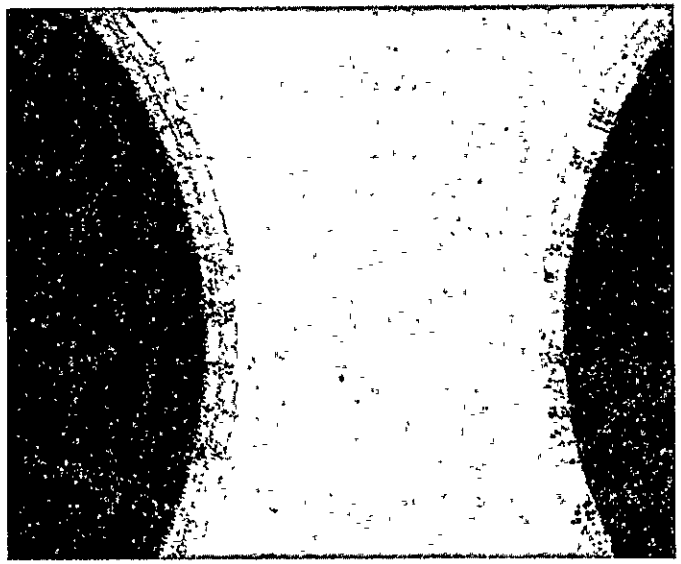

1000X-OM

	Counts Above Background*					
Elem/Area	A	B	C	D	E	F
Al kα	134	--	--	--	--	--
Si kα	--	600	60	940	175	3260
Ti kα	512	2786	3860	3700	2880	3600
Cr kα	2480	3567	130	337	65	160
Fe kα	132	30	20	280	50	5530
Co kα	1143	414	16	963	110	1336
Ni kα	3615	1700	90	2500	220	3514
Zr kα	33	1300	200	--	--	--

*4000 cts in max channel

Fig. 19. Energy Dispersive X-ray Analysis of Interface Between TiN Coated SiC Fibers and Waspaloy Matrix as-HIP 2 Hours at 996°C (1825°F), 103 MPa (15,000 psi).

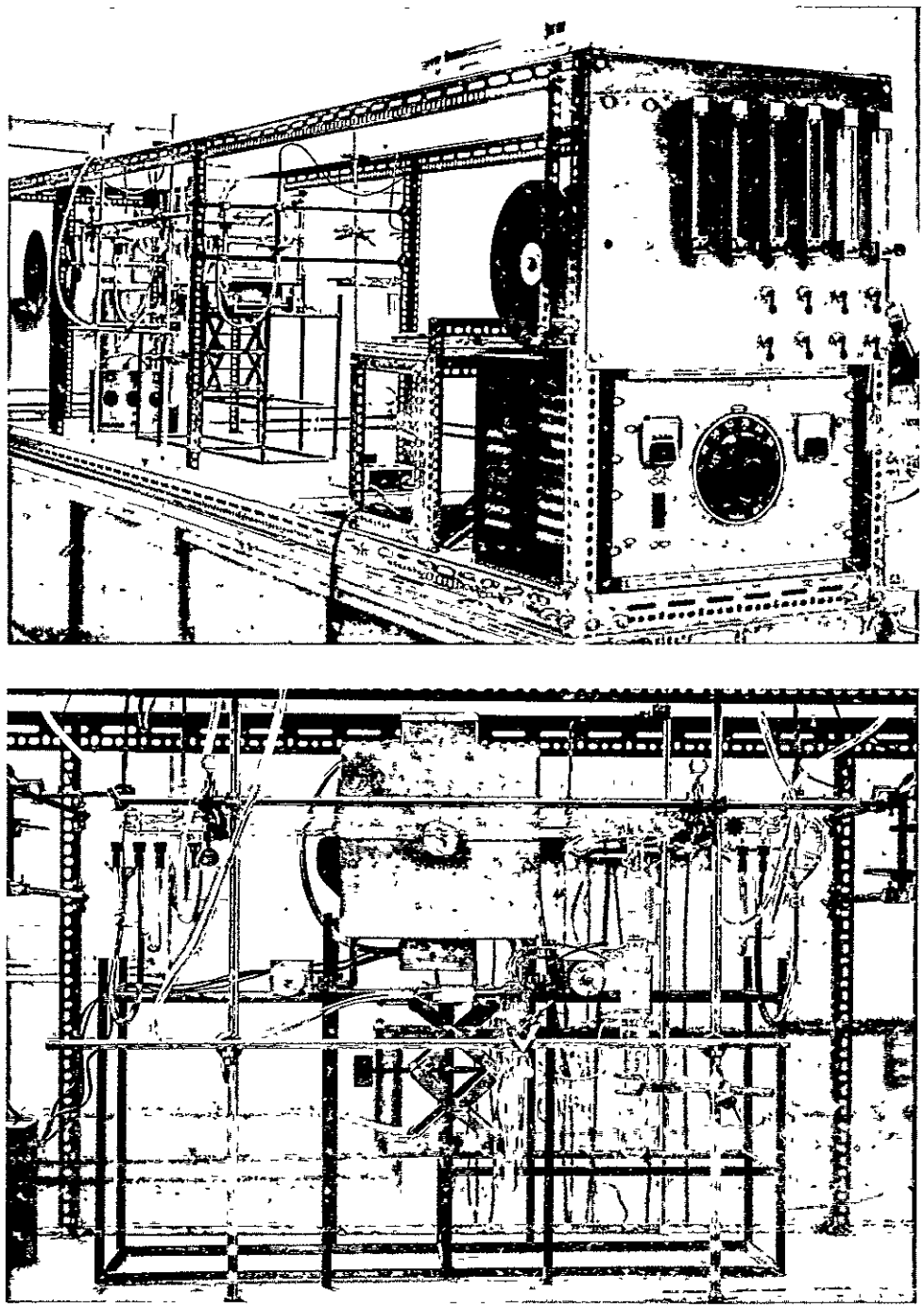

Fig. 20. CVD Apparatus for Depositing Refractory Metal Carbides and Nitrides on SiC Filament.

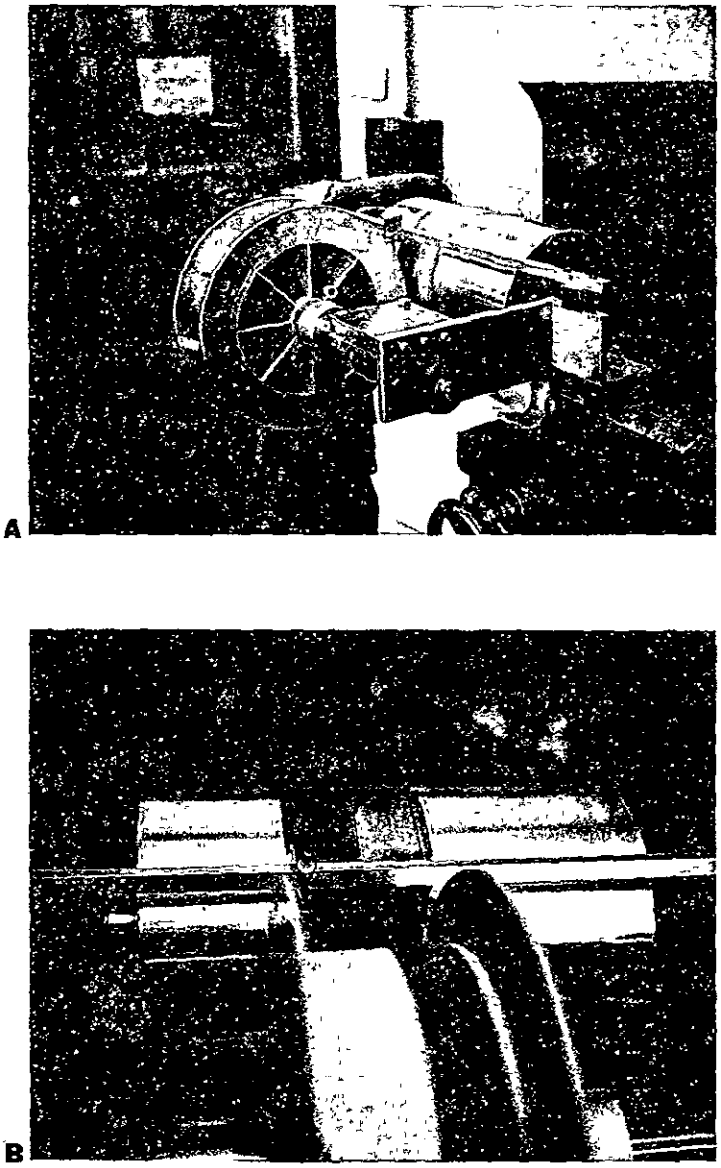

Fig. 21. Filament Winding Apparatus.

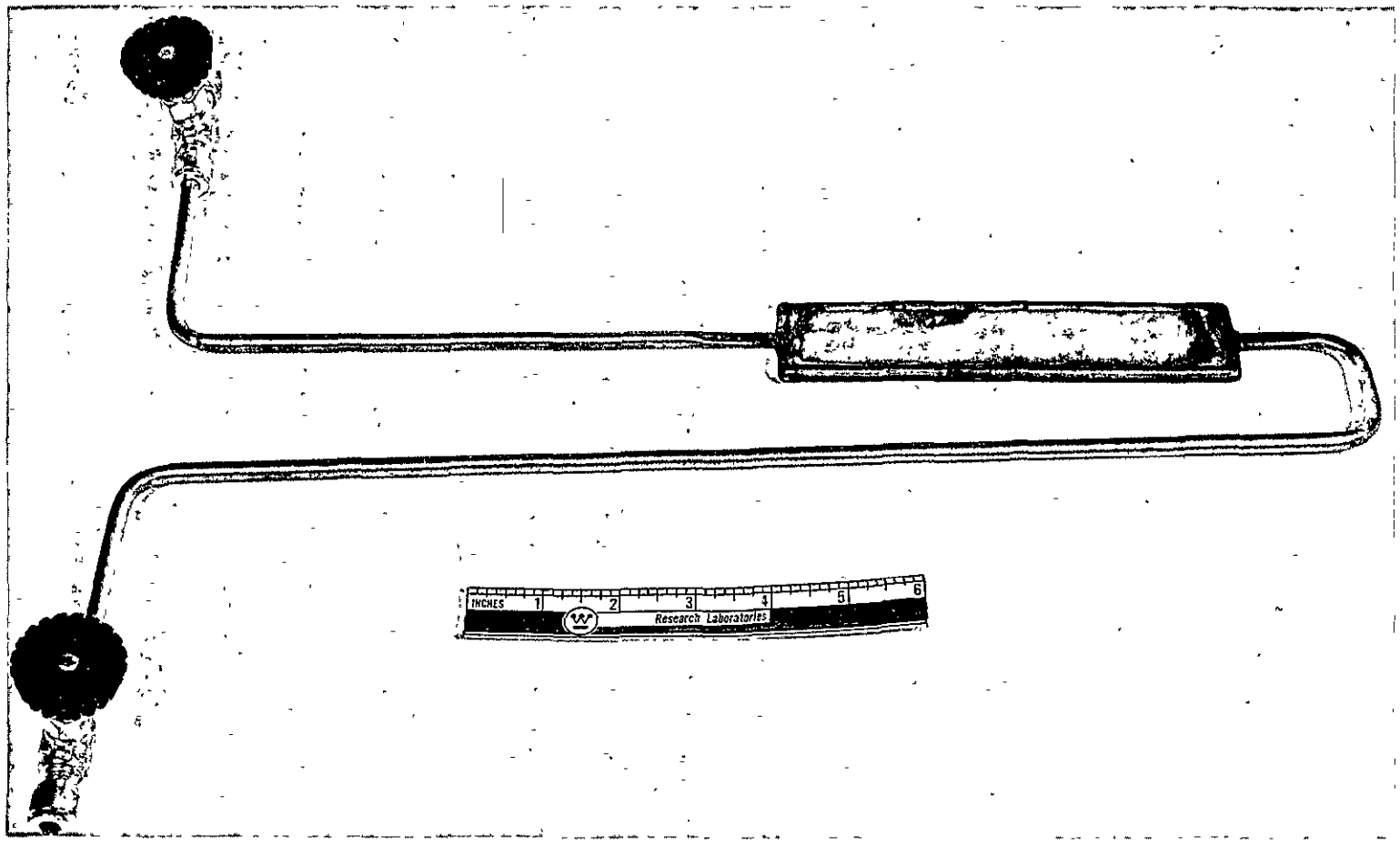

Fig. 22. HIP capsule prior to binder removal, evacuation, and forge sealing.

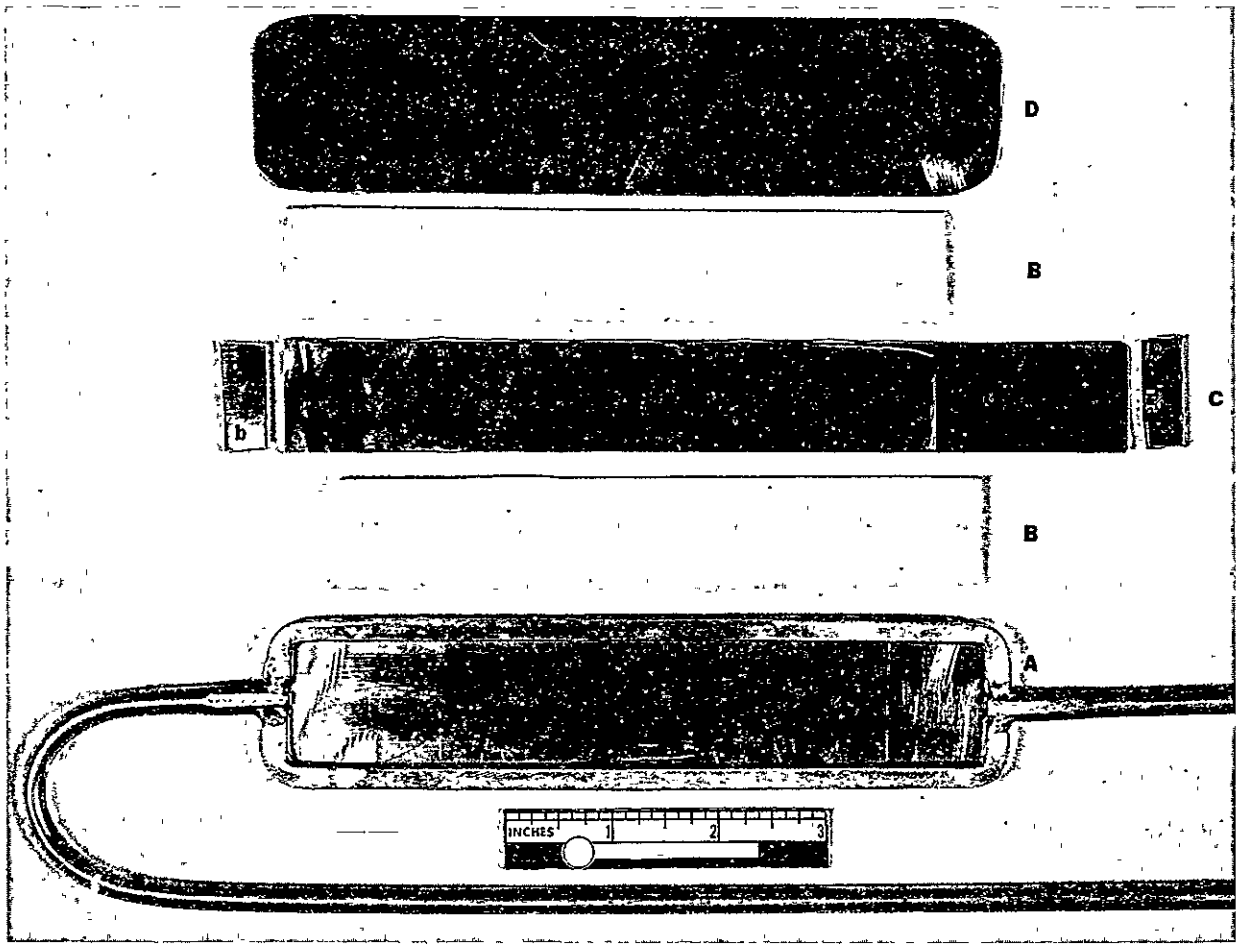

A. Picture frame can with inlet and exit pinch-off tubes
B. Parting agent - refractory felt
C. Composite bundle with (a) Waspaloy foil liner, (b) end clips, and (c) powder tape and SiC green layup.
D. Top cover

Fig. 23. Layup Assembly for Composite Mini-Panels.

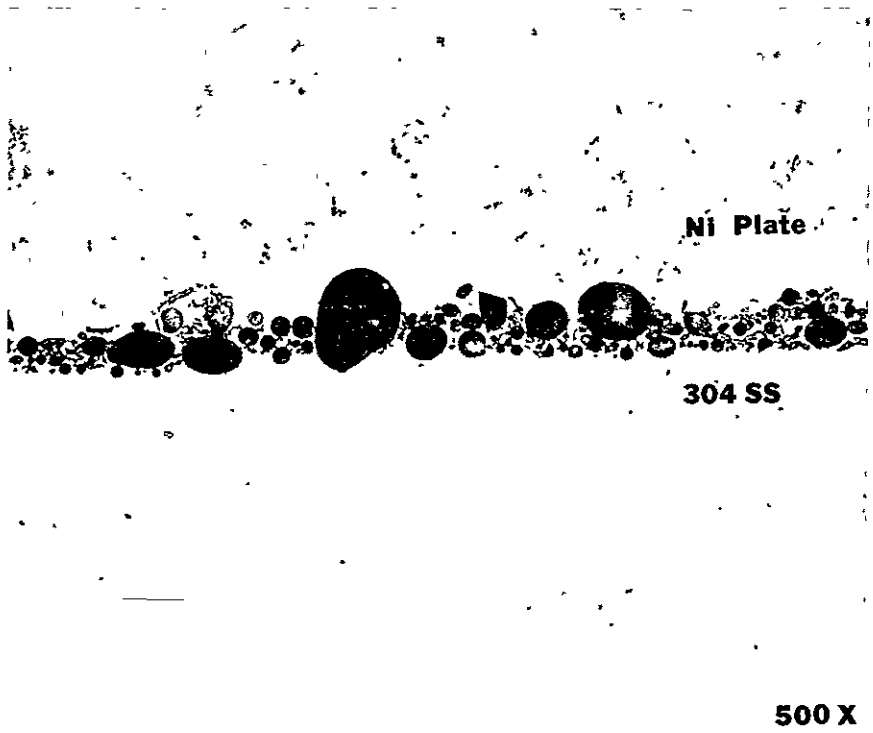

Fig. 24. Fiberfrax Refractory Felt Remnants Imbedded in 304 Cover Plate After Parting From Waspaloy Composite After HIP at 996°C (1875°F) 2 Hours at 138 MPa (20 ksi).

Fig. 25. Post HIP Can #8S80-5 After Separation of Top and Bottom HIP Enclosures (A & B From Composite Panel C). Dark Color is Due to Parting Compound.

Fig. 26. Radiographs of HIP Panel 8S80-5 Prior to Decanning.

Fig. 27. Cross Section of Composite Panel 8S80-5A. Note Numerous Areas of Interaction Between Fiber and Matrix.

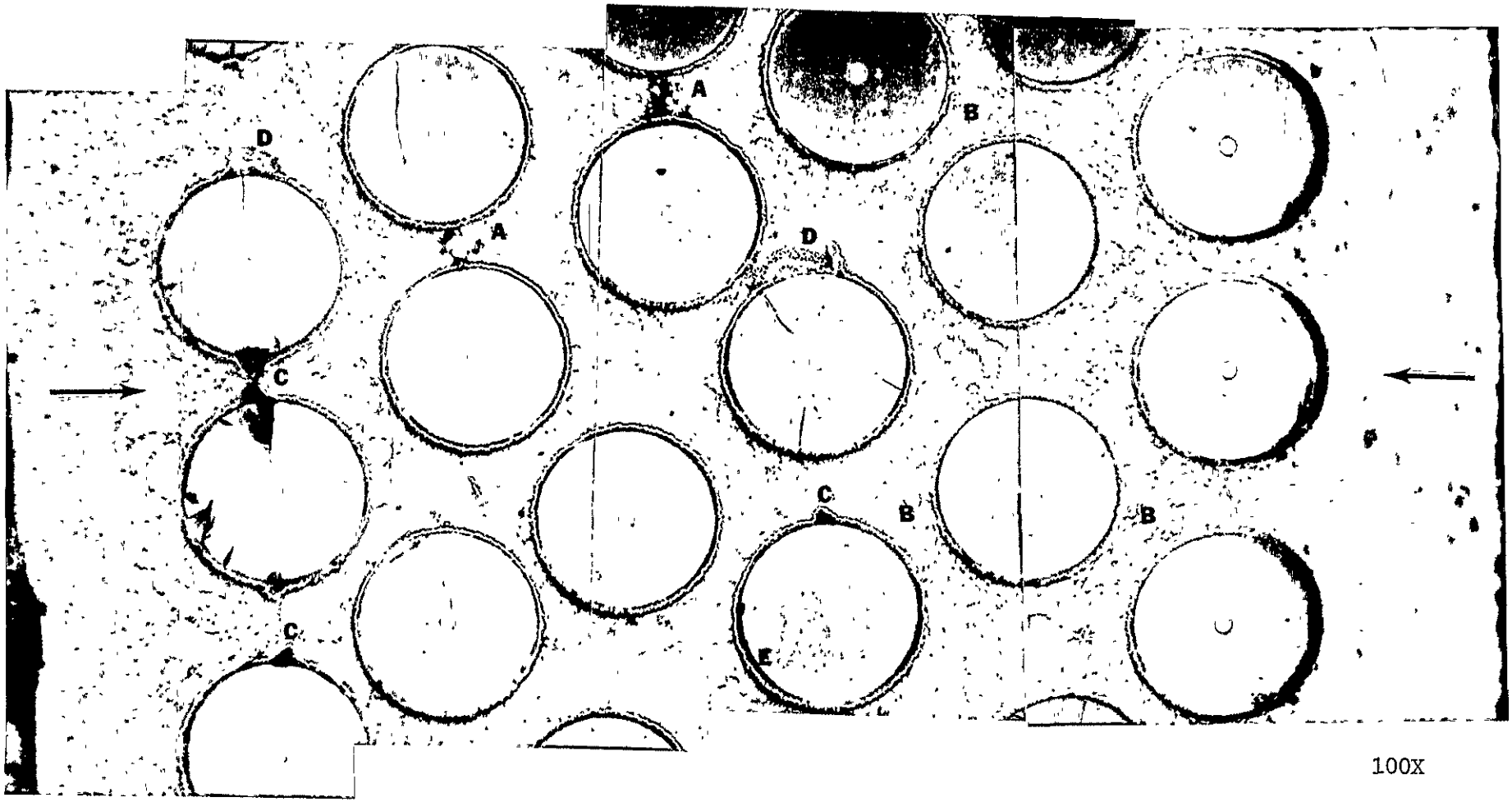

Fig. 28. Cross Section of Head Section of Specimen 8S80-5A.
Etchant: Electrolytic - 10% Chromic Acid.

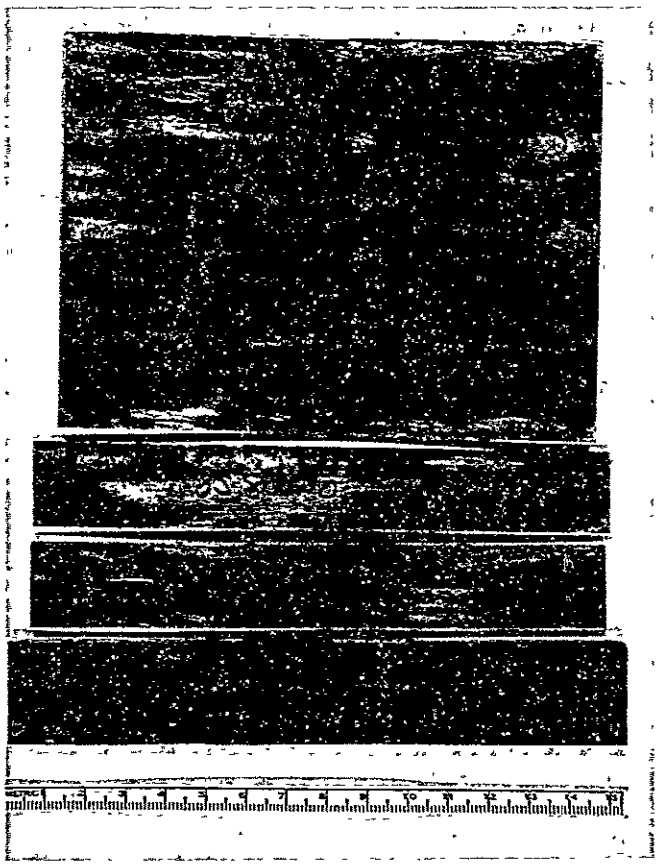

Fig. 29. Uniaxial, Six Ply, 55 v/o Tungsten Coated SiC/Waspaloy Composite Panels.

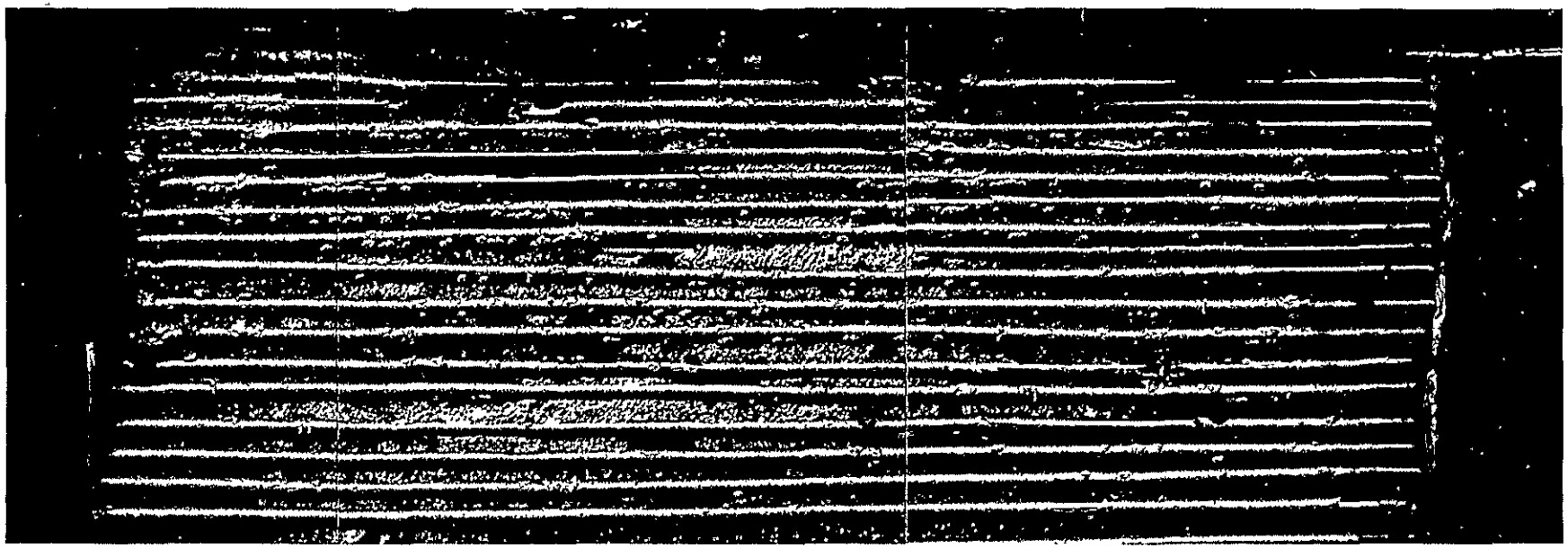

20X

Fig. 30. Electrolytically Exposed Filament in as HIP Panel No. P154. Note Growth of Interaction "Blooms" at Coating Defects on Filament Surface.

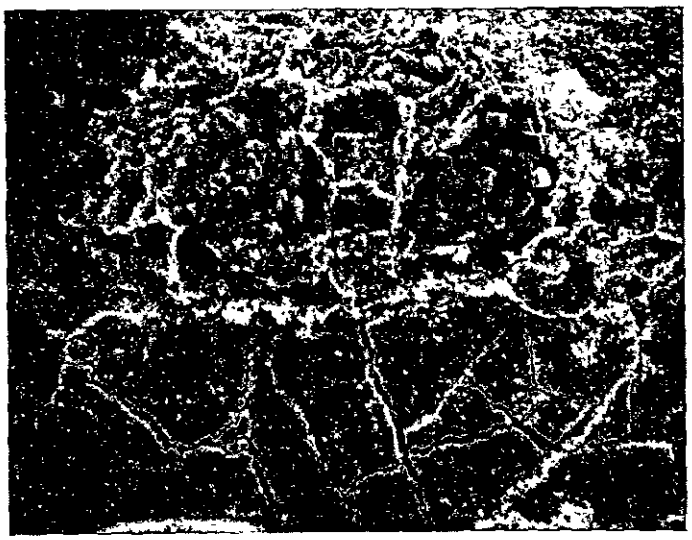

Fig. 31. SEM Photographs of "Blooms" on the Surface of Electrolytically Exposed HfC Coated SiC Filament From Composite Panel P-154.

KEV	Rad	Cts
0.83		66P
1.71	Si-Kα	897P
2.32	Mo-Lα	540P
2.59		156P
4.50	Ti-Kα	615P
5.40	Cr-Kα	3215P
5.94	Cr-Kβ	422P
6.89	Co-Kα	495P
7.45	Ni-Kα	2048P
8.23	Ni-Kβ	256P

Area A

KEV	Rad	Cts
0.73		181P
1.66	Hf-Mα	3080P
2.06		51P
2.31		67P
4.50	Ti-Kα	430P
5.40	Cr-Kα	475P
5.88		33P
6.89		97P
7.44	Ni-Kα	279P
7.86	Hf-Lα	694P
8.99	Hf-$L\beta_1$	298P
9.29	Hf-$L\beta_2$	175P
10.48	Hf-$L\gamma_1$	21P

Area B

KEV	Rad	Cts
1.31		208P
1.65	Hf-Mα	3129P
2.09		101P
4.48		232P
5.39		42P
6.90		16P
7.85	Hf-Lα	821P
8.97	Hf-$L\beta_1$	329P
9.24	Hf-Lβ	159P
10.47	Hf-Lγ	40P
18.25		4P

Area C

KEV	Rad	Cts
0.84		50P
1.55	Al-Kα	62P
2.16	Au-Mo	1260P
2.87	Pd-Lβ	747P
4.49	Ti-Kα	294P
5.39	Cr-Kα	2150P
5.94	Cr-Kβ	218P
6.89	Co-Kα	885P
7.44	Ni-Kα	3333P
8.22	Ni-Kβ	417P
9.66	Au	229P
11.43	Au	85P

General Matrix (Waspalloy) from Metallographic Section of P-154

KEV	Rad	Cts
1.40		26P
1.74	Si-Kα	3401P
2.14	Au	304P
2.86	Pd	181P
8.07		14P
9.65		55P
11.40		20P

SiC Filament from Metallographic Section of P-154

500X

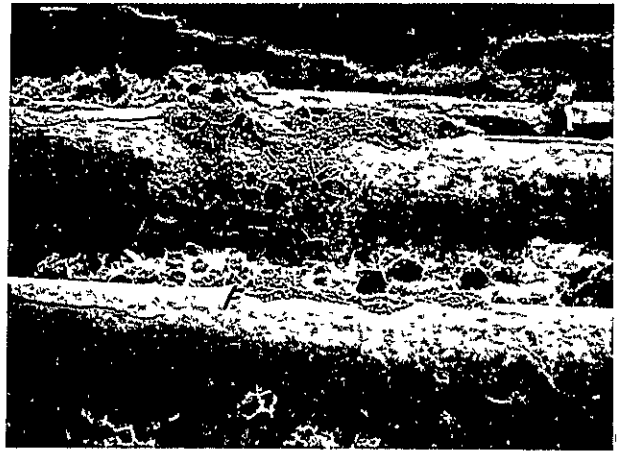

250X

Fig. 32. Energy Dispersive X-ray Analysis of Filament Surface Features From Composite Panel P-154.

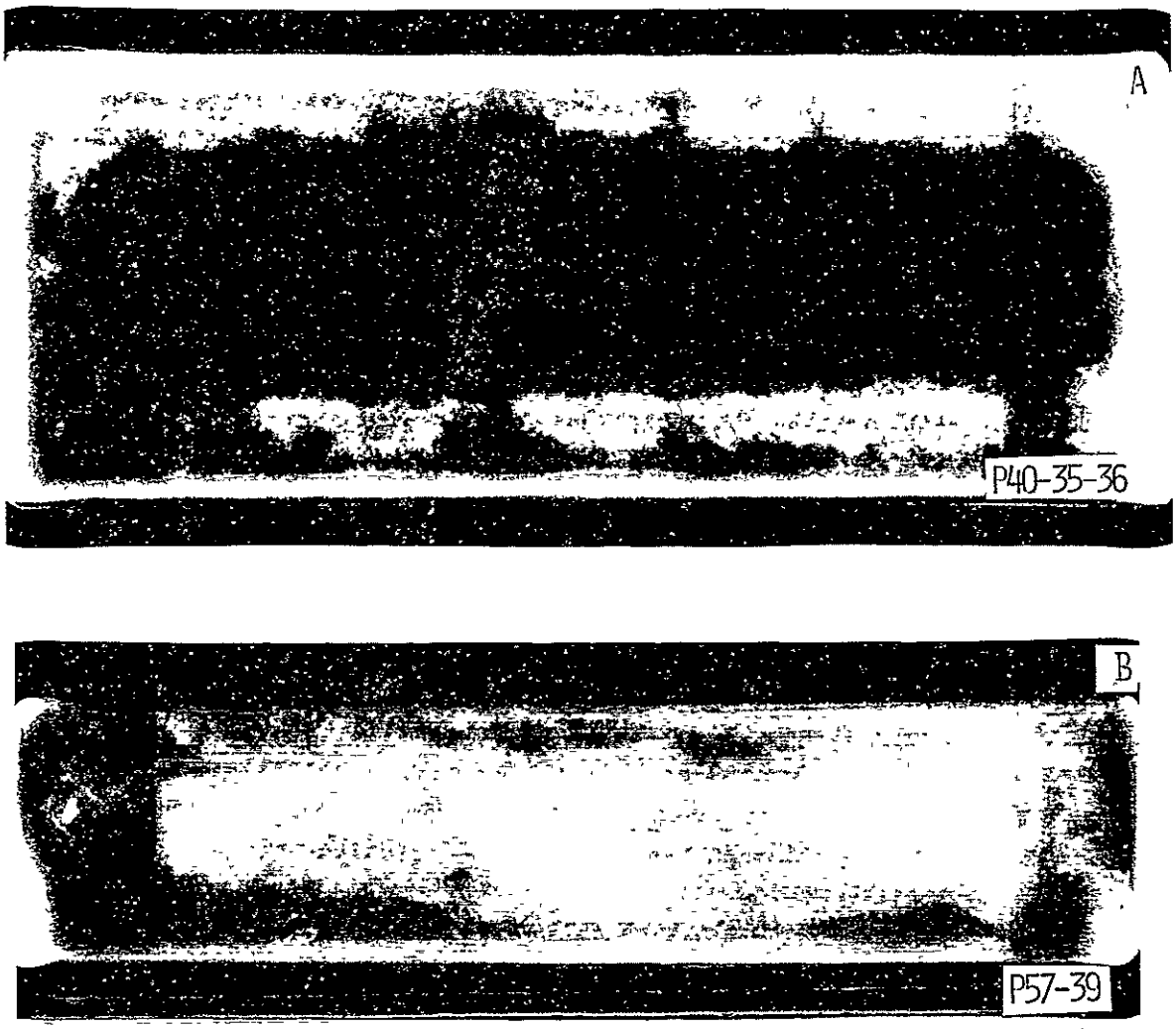

Fig. 33. Radiographs of Composite Panels Prior to HIP Envelope Removal.

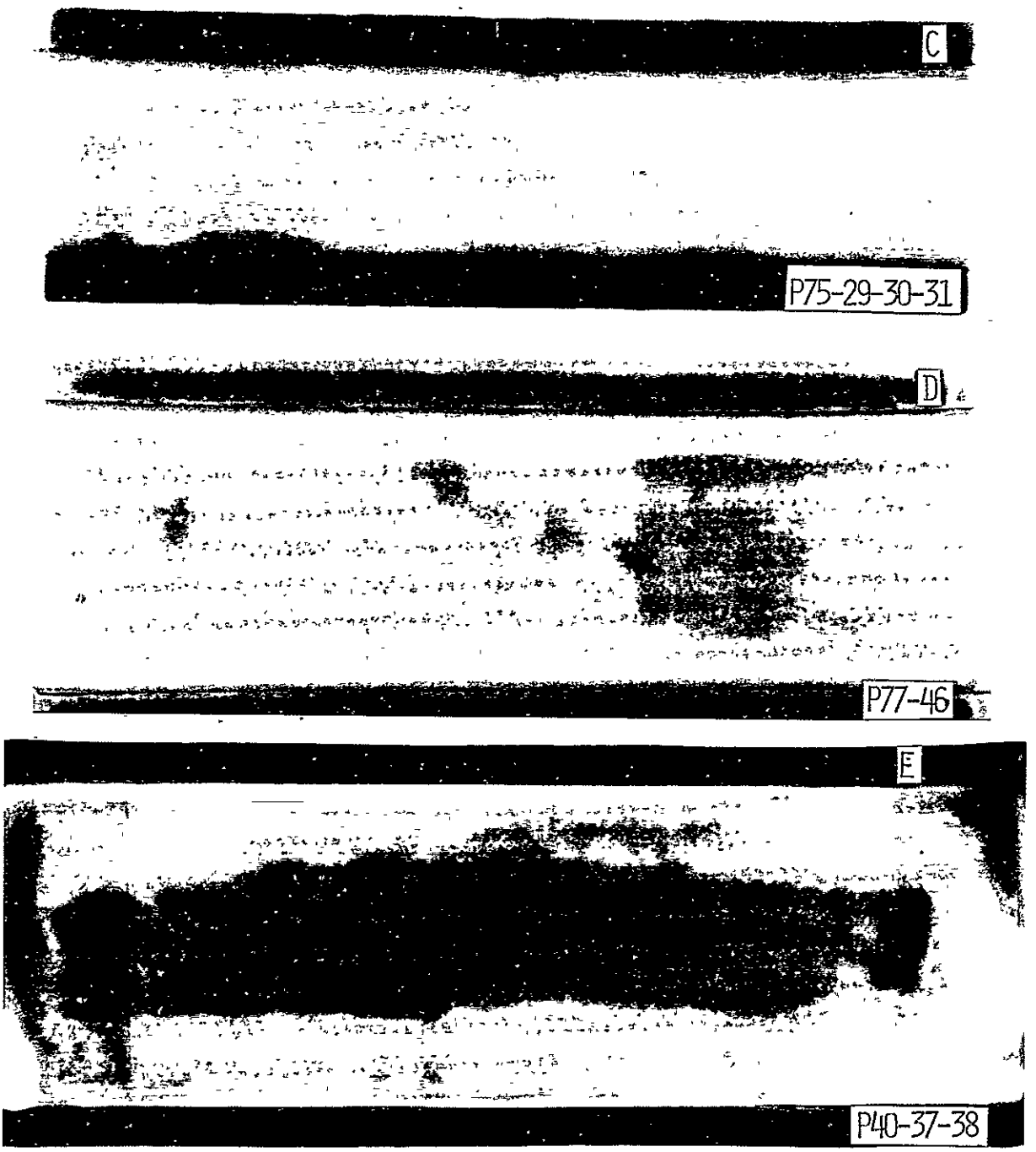

Fig. 33(Continued) Radiographs of Composite Panels Prior to HIP Envelope Removal.

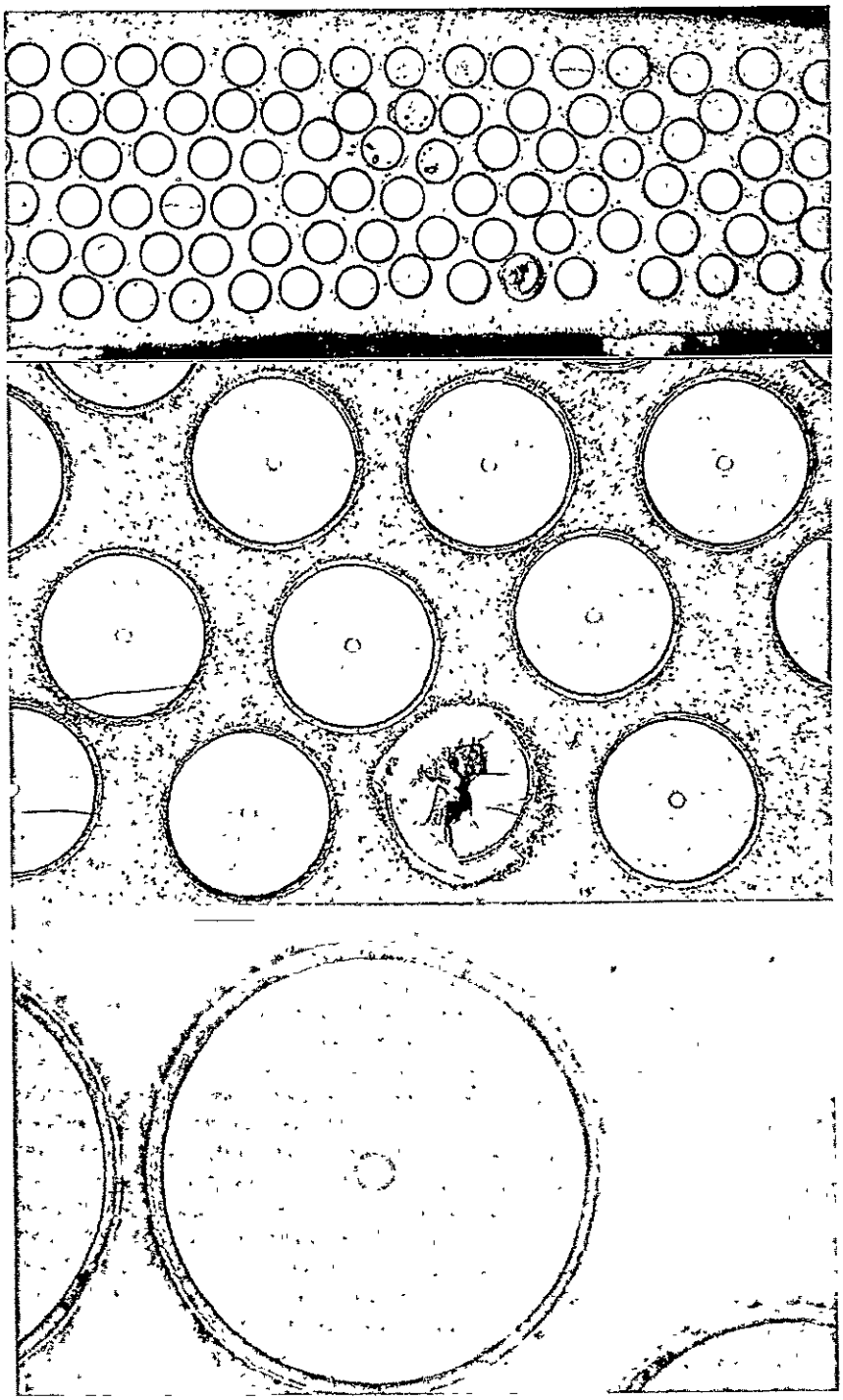

Fig. 34. As HIP (P40-38) Cut From Between Specimens P40-58 #1A #1B

Q-437

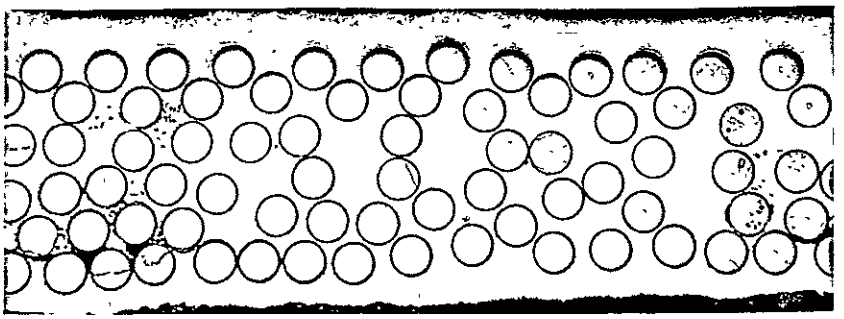

50X

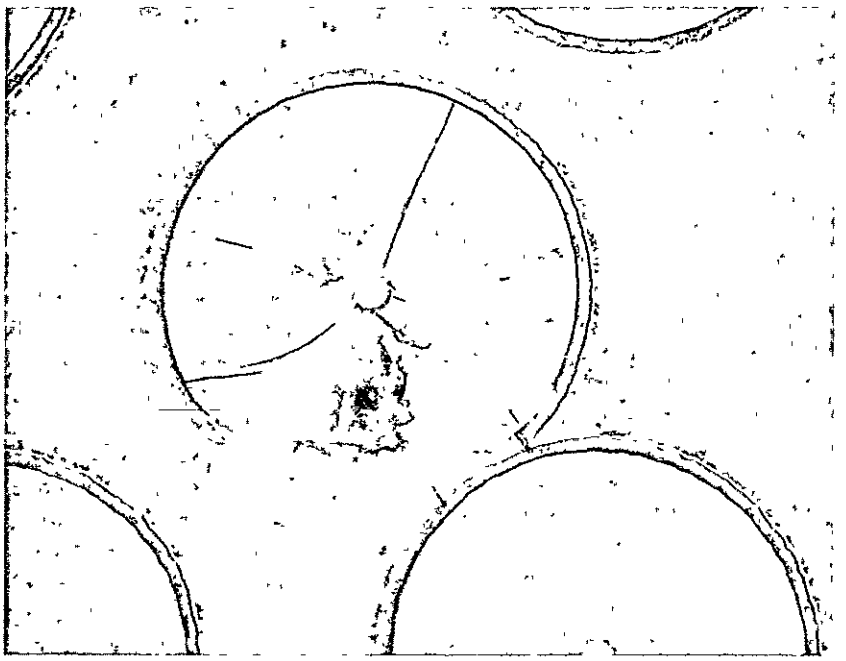

500X

Fig. 35. - As HIP (P40-38) Cut From Between Edge Specimen P40-38 #4A #4B Q-438

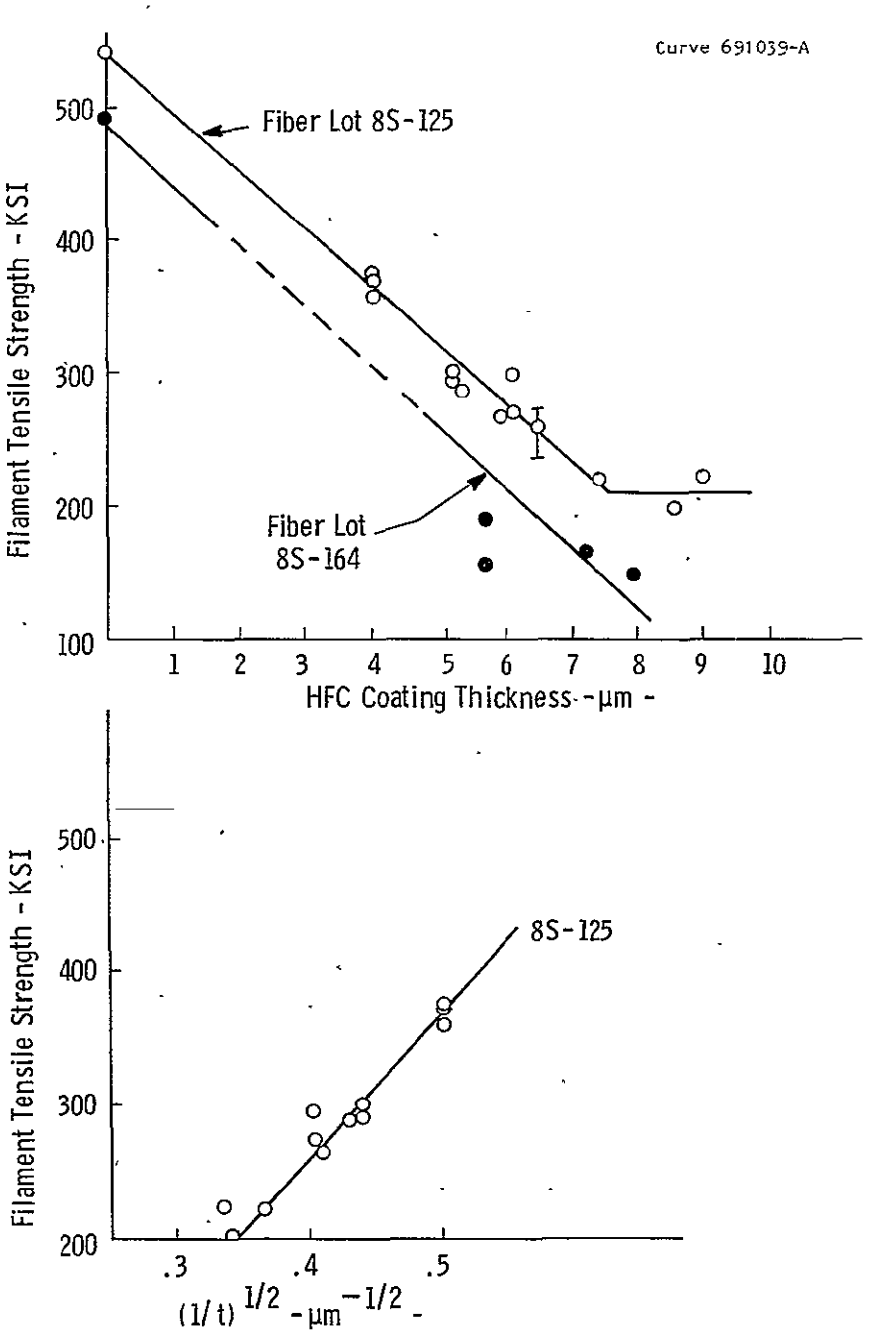

Fig. 36. Variation of Room Temperature Tensile Strength With CVD-HfC Thickness

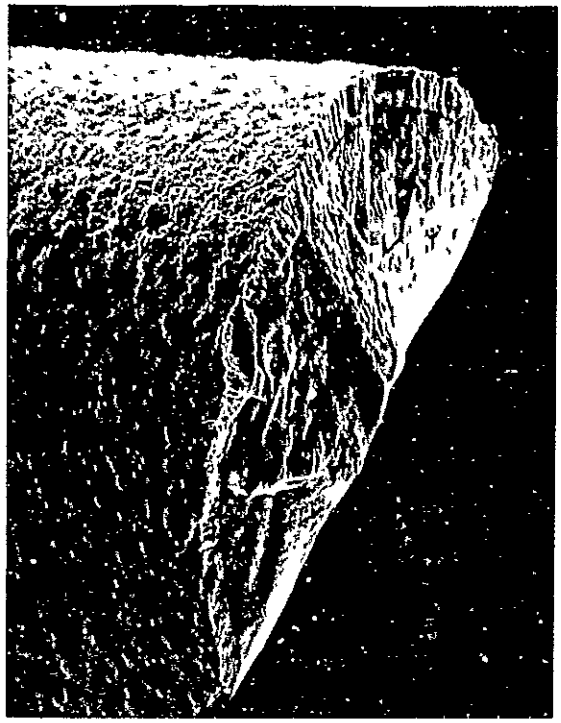

600X

600X

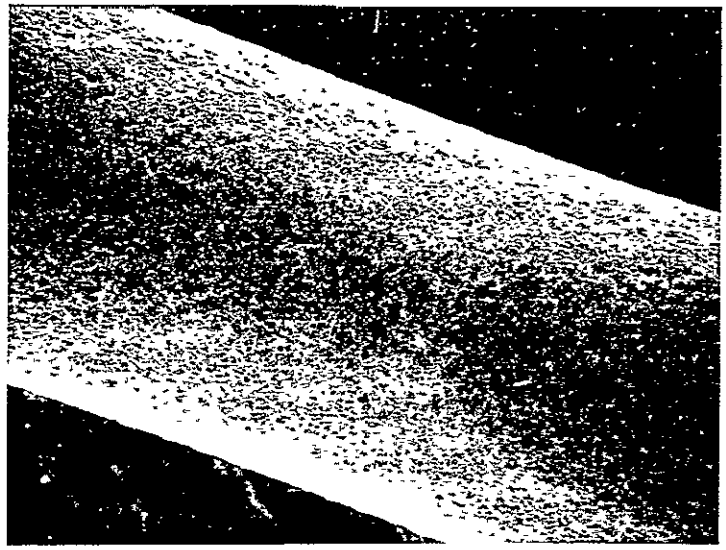

300X

Fig. 37. SEM Photographs of CVD HfC Coated SiC Filament. Fiber Lot 85-125 - Run No. 31.

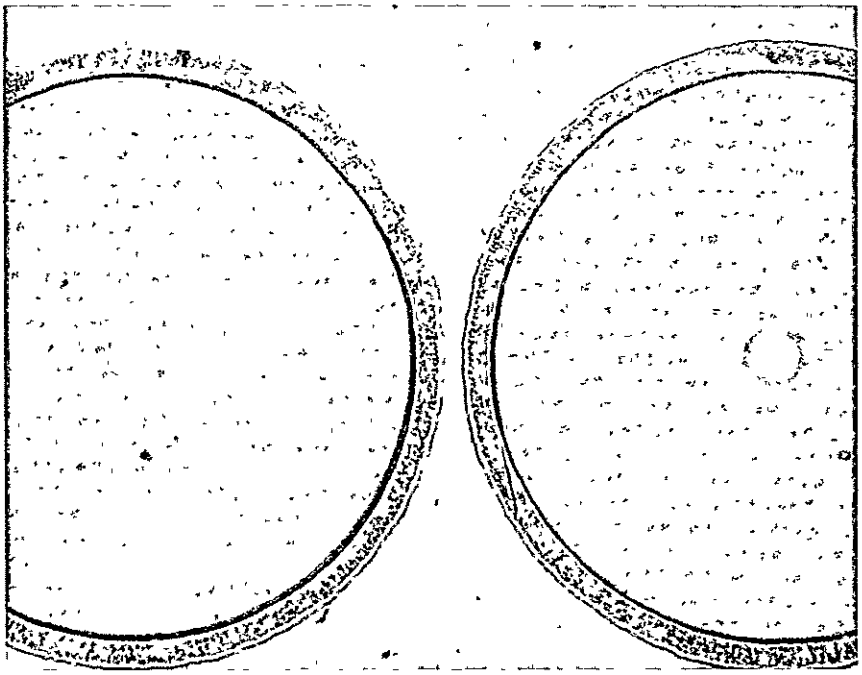

500X

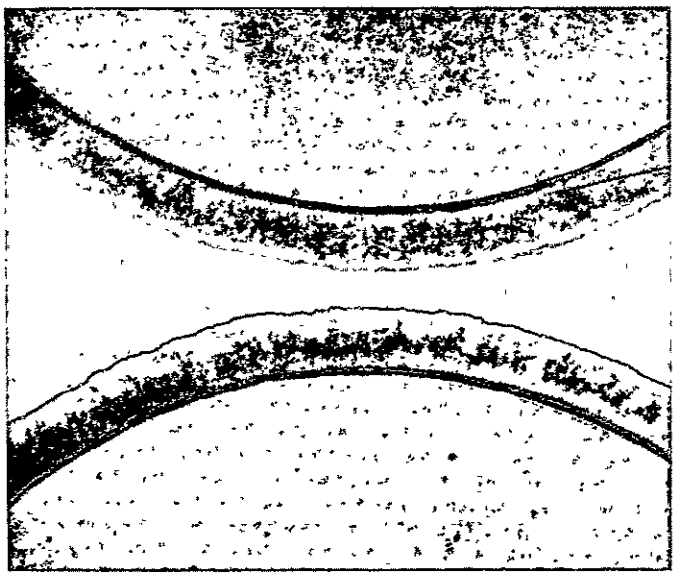

1000X

Fig. 38. CVD HfC Run No. 38f on SiC Lot 85-125. As Coated and Ni Plated.

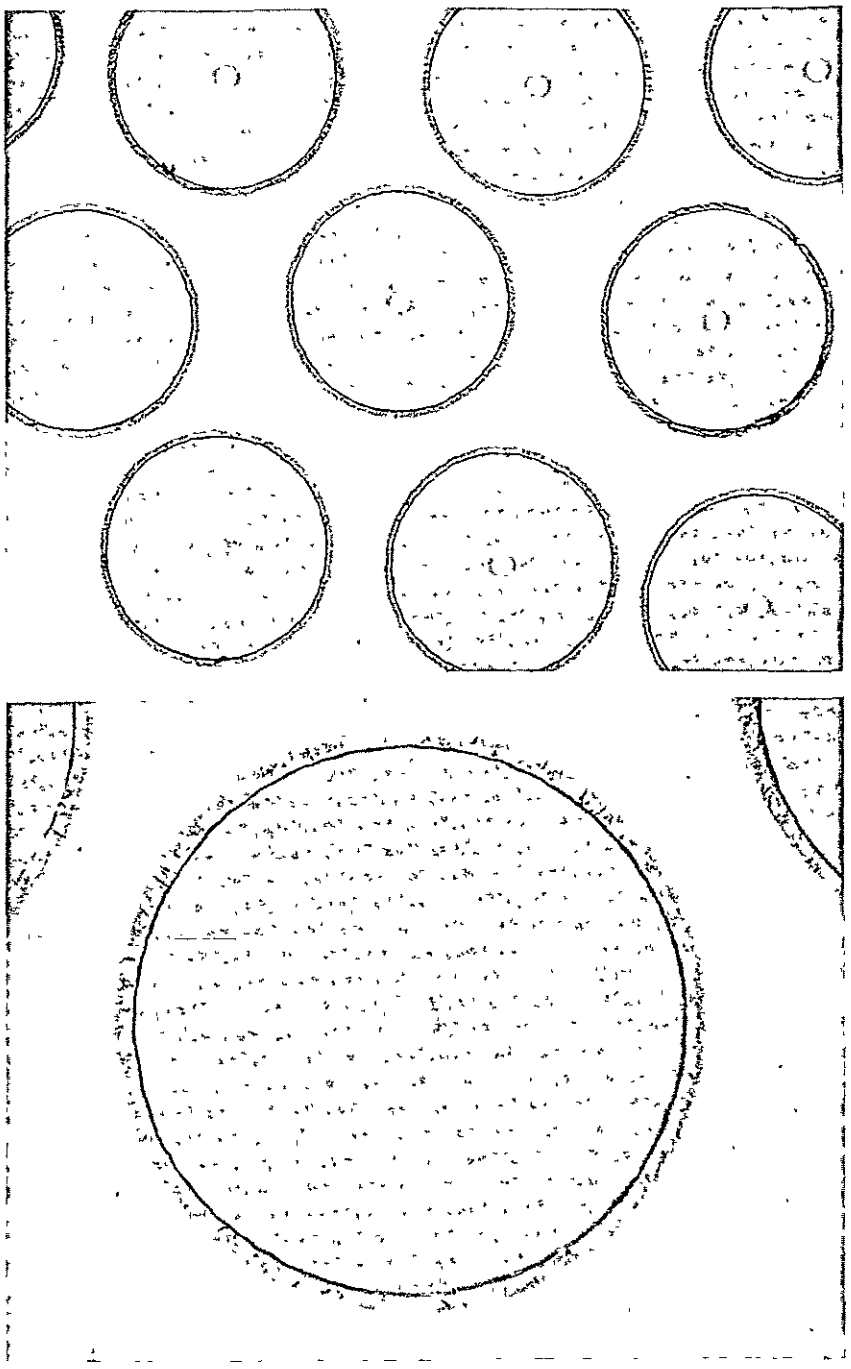

Fig. 39. Microstructure of Central Region of P40-38.

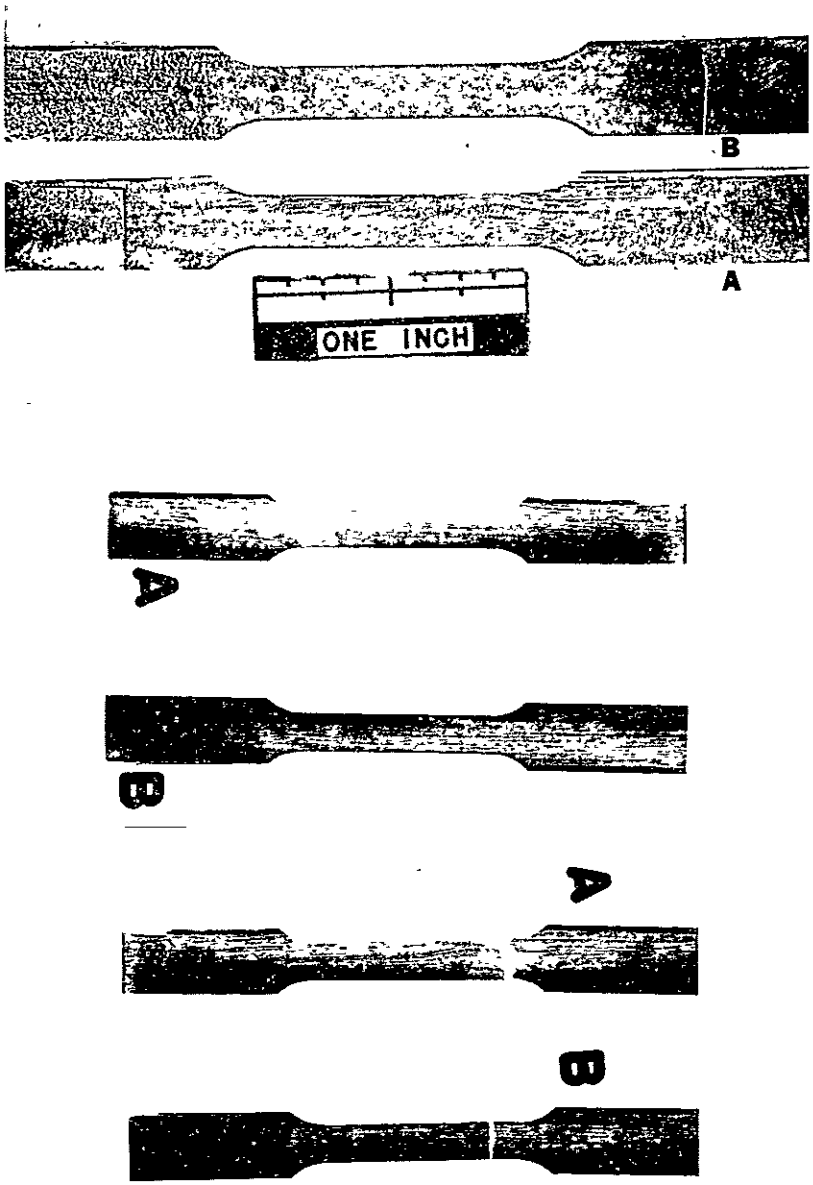

Fig. 40. Room Temperature Tensile Specimens 8S80-5A and B With Pre- and Post-Test Radiographs

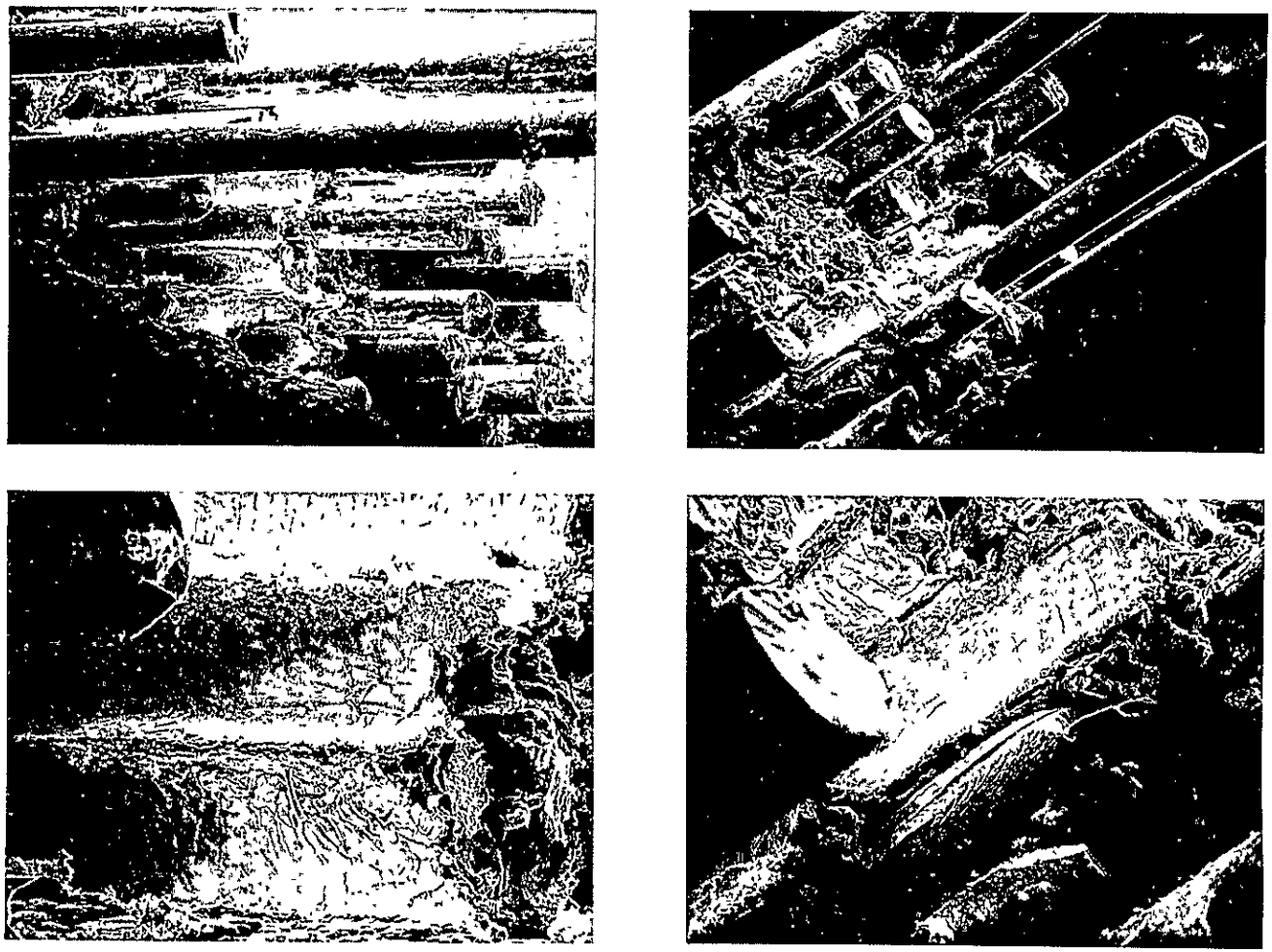

Fig. 41. Fracture Surfaces of HfC Coated SiC/Waspalloy Composite P-154 After Tensile Testing at Indicated Temperatures

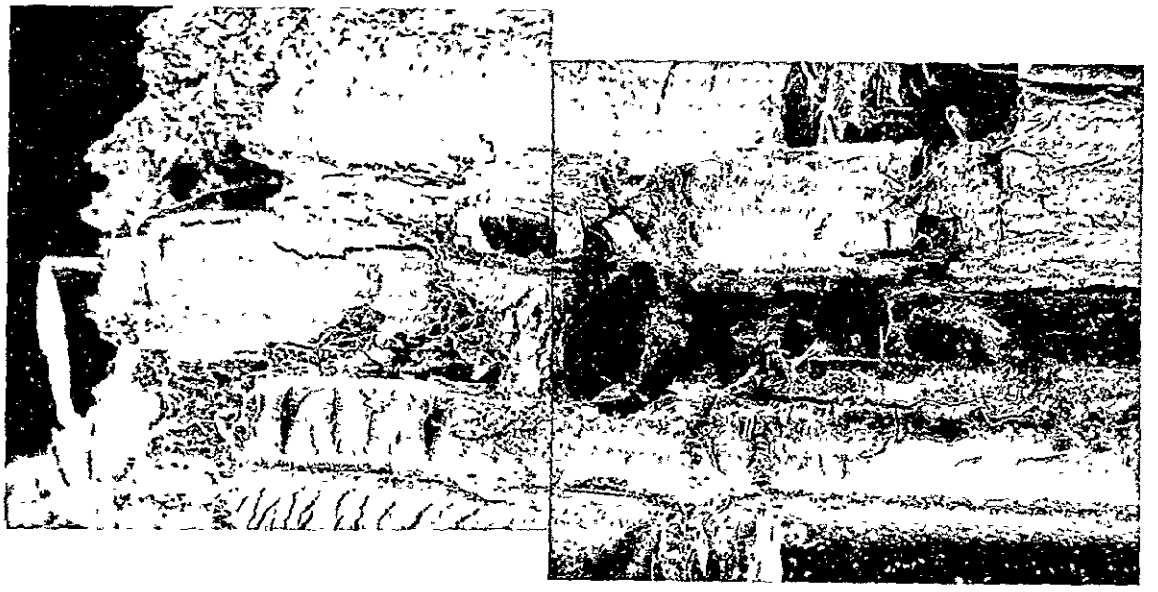

200X

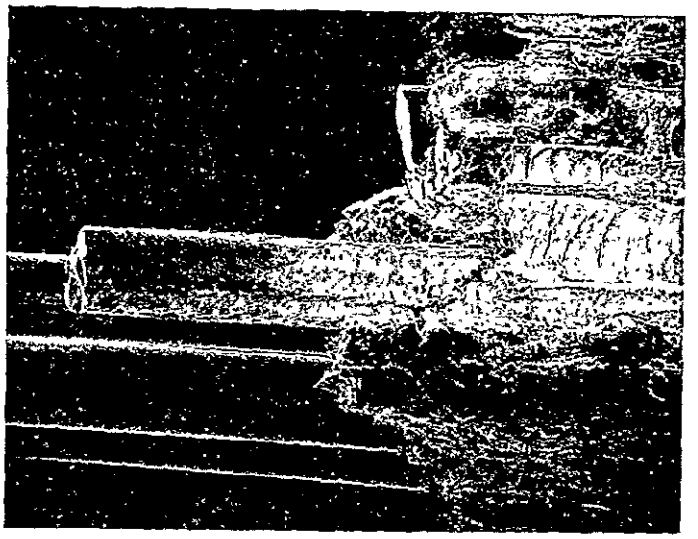

100X

Fig. 42. Fracture Surface of Specimen P40-38-2 After Tensile Testing at 982°C (1800°F).

NASA-Johnson Space Center
Houston, TX 77058
Attn: Library-Code JM6 (1)

Jet Propulsion Laboratory
4800 Oak Grove Drive
Pasadena, CA 91102
Attn: Library (1)

Defense Documentation Center
Cameron Station
5010 Duke Street
Alexandria, VA 22314 (2)

Department of the Air Force
Air Force Materials Lab
Wright-Patterson AFB, OH 45433
Attn: B. Kosmal (1)

Department of the Air Force
Air Force Materials Lab
Wright-Patterson AFB, OH 45433
Attn: S. R. Lyon (LLM) (1)

Department of the Air Force
Air Force Materials Lab
Wright-Patterson AFB, OH 45433
Attn: E. Joseph (LLC) (1)

Department of the Army
Army Air Mobility R&D Lab
Fort Eustis, VA 23604
Attn: J.White(SAVDL-EU-TA) (1)

Department of the Army
Maags Research Center
Watervliet Arsenal
Watervliet, NY 12189
Attn: I. Ahmad (1)

Department of the Navy
Bureau of Naval Weapons
Washington, DC 20525
Attn: T. F. Kearns (RRMA-2) (1)

NASA Scientific & Tech.
Information Facility (10)
P.O. Box 8757
Balt/Wash Int. Airport, MD 21240

MMIC
Battelle Memorial Institute
505 King Avenue
Columbus, OH 43201 (1)

Department of the Air Force
Air Force Materials Lab
Wright-Patterson AFB, OH 45433
Attn: V. DiBenedetto (LTN) (1)

Department of the Air Force
Air Force Materials Lab
Wright-Patterson AFB, OH 45433
Attn: W. A. Schulz (LC) (1)

Department of the Air Force
AFAPL/TBP
Wright-Patterson AFB, OH 45433
Attn: T. Norbut (1)

Department of the Army
AMMRC
Watertown, MA 02172
Attn: A. P. Levitt (1)

Inst. for Defense Analysis
Science & Technology Div.
400 Army-Navy Drive
Arlington, VA 22202
Attn: E. L. Foster (1)

Department of the Navy
NASC AIR 52/03
Washington, DC 20360
Attn: R. Schmidt (1)

Department of the Navy
Naval Surface Weapons Center
White Oak, MD 20910
Attn: A. P. Divecha (WR-32) (1)

Department of the Navy
NASC Air-52031B
Washington, DC 20361
Attn: I. Machlin (1)

National Bureau of Standards
Inst. for Applied Technology
Bldg. 225, Room B-105
Washington, DC 20234
Attn: K. G. Kreider (1)

Amercom, Inc.
9060 Winnetka Ave.
Northridge, CA 91324
Attn: G. W. Burt (1)

AVCO Corporation
Lycoming Division
550 South Main Street
Stratford, CT 06497
Attn: B. Goldblatt (1)

Battelle Memorial Institute
505 King Avenue
Columbus, OH 43201
Attn: K. R. Handby (1)

Bell Aerosystems Company
P. O. Box 1
Buffalo, NY 14205
Attn: Engineering Lab (1)

COMSAT Laboratories
Materials Technology Branch
Clarksburg, MD 20734
Attn: L. Sparrow (1)

Drexel University
Department of Metallurgy
Philadelphia, PA 19104
Attn: A. Lawley (1)

Fiber Materials, Inc.
Biddeford Industrial Park
Biddeford, ME 04005
Attn: R. T. Pepper (1)

Aerospace Corporation
P.O. Box 92957
Los Angeles, CA 90009
Attn: G. Kendall (1)

AVCO Corporation
Lowell Industrial Park
Lowell, MA 01850
Attn: J. Henshaw (1)

Battelle Memorial Institute
505 King Avenue
Columbus, OH 43201
Attn: B. Noten (1)

Battelle Memorial Institute
505 King Avenue
Columbus, OH 43201
Attn: Library (1)

Boeing Company
P. O. Box 733
Renton, WA 98055
Attn: W. E. Benz (1)

Dolowy-Webb Associates
22072 Rayen Street
Canoga Park, CA 91304
Attn: J. F. Dolowy, Jr. (1)

E. I. duPont de Nemours & Co.
Textile Fibers Department
Wilmington, DE 19898
Attn: C. Zweben (B262/Rm 433) (1)

General Dynamics/Convair
P. O. Box 748
Fort Worth, TX 76101
Attn: Tech. Library (6212) (1)

General Electric Co.
Adv. Engine & Tech. Programs
Cincinnati, OH 45212
Attn: R. Stabrylla (1)

General Dynamics/Convair
P. O. Box 1128
San Diego, CA 92112
Attn: N. R. Adsit (1)

General Electric Co.
Adv. Engine & Tech. Programs
Cincinnati, OH 45212
Attn: M.A.Zipkin (H-44) (1)

General Electric Co.
Mat. & Proc. Technology Labs.
Cincinnati, OH 45215
Attn: R. Carlson (1)

General Electric Co.
Valley Forge Space Tech. Center
P. O. Box 8555
Philadelphia, PA 19101
Attn: L. R. McCreight (1)

General Motors Corp.
Detroit Diesel-Allison Div.
Materials Laboratory
Indianapolis, IN 46206
Attn: M. Herman (1)

Grumman Aircraft Eng. Corp.
Bethpage, NY 11714
Attn: W. Wolkowitz (1)

IIT Research Institute
Technology Center
10 West 35th Street
Chicago, IL 60616
Attn: Tech. Library (1)

Lockheed-Georgia Co.
Marietta, GA 30060
Attn: Tech. Library (1)

Lockheed Missiles & Space Co.
111 Lockheed Way
Sunnyvale, CA 94088
Attn: M. I. Jacobson (B-150) (1)

General Electric Co.
Adv. Engine & Tech. Programs
Cincinnati, OH 45212
Attn: A. Adamson (1)

General Electric Co.
Mat. & Proc. Technology Labs.
Cincinnati, OH 45212
Attn: Library (1)

General Electric Co.
Advanced Technology Lab.
Schenectady, NY 12305
Attn: Library (1)

Gould Inc.
Engine Parts Division
17000 St. Clair Avenue
Cleveland, OH 44110
Attn: G. R. Kingsbury (1)

Airesearch Div.-Garrett Corp.
402 S. 36th Street
Phoenix, AZ 85034
Attn: D. J. Tree (1)

Lehigh University
Department of Metallurgy
Bethlehem, PA 18015
Attn: R. W. Kraft (1)

Lockheed-Palo Alto Res. Lab.
Materials & Scientific Lab.
3251 Hanover Street
Palo Alto, CA 94303
Attn: W. Bradshaw (1)

P. R. Mallory Company
Northwest Industrial Park
Burlington, MA 01803
Attn: R. H. Krock (1)

McDonnel-Douglas Astronautics
M&P Development
Dept. 247, Bldg. 32
St. Louis, MO 63166
Attn: G. B. Bilow (1)

Martin-Marietta Corp.
P. O. Box 5837 MP 129
Orlando, FL 32805
Attn: R. A. Mayor (1)

Midwest Research Institute
425 Volker Blvd.
Kansas City, MO 61110
Attn: J. R. Hancock (1)

Rensselaer Polytechnic Inst.
Materials Engineering Dept.
Troy, NY 12181
Attn: R. J. Diefendorf (1)

Rockwell International
Los Angeles Division
International Airport
Los Angeles, CA 90045
Attn: C. Hamilton (SB08) (1)

Sandia Corporation
P. O. Box 5800
Albuquerque, NM 87115
Attn: D. M. Schuster - 5840 (1)

Dr. E. Scala
Consulting Engineer
P. O. Box 1362
Cortland, NY 13045 (1)

Southwest Research Institute
8500 Culebra Rd - Box 28510
San Antonio, TX 78284
Attn: G. C. Grimes (1)

TRW Equipment Laboratories
Materials Technology
23555 Euclid Avenue
Cleveland, OH 44117
Attn: I. J. Toth (1)

TRW Equipment Laboratories
Materials Technology
23555 Euclid Avenue
Cleveland, OH 44117
Attn: P. Melnyk (1)

NETCO
2225 E. 28th St. (Bldg. 5)
Long Beach, CA 90806
Attn: L. W. Davis (1)

Rockwell International
Space Division
12214 Lakewood Blvd.
Downey, CA 90241
Attn: A. J. Yeast (1)

Rockwell International
P. O. Box 1259
4300 E. Fifth Avenue
Columbus, OH 43216
Attn: Tech. Library (1)

Sandia Corporation
P. O. Box 5800
Albuquerque, NM 87115
Attn: W. R. Hoover - 5844 (1)

Solar Div. - Int. Harvester
2200 Pacific Coast Highway
San Diego, CA 92138
Attn: A. G. Metcalfe (1)

TRW Systems Group
One Space Park
Redondo Beach, CA 90278
Attn: A. Toy (1)

TRW Equipment Laboratories
Materials Technology
23555 Euclid Avenue
Cleveland, OH 44117
Attn: G. Doble (1)

Union Carbide Corp.
Parma Technical Center
P. O. Box 6116
Cleveland, OH 44101
Attn: R. V. Sara (1)

United Technologies Corp.
Pratt & Whitney Div.
E. Hartford, CT 06108
Attn: Tony Dennis (1)

United Technologies Corp.
Pratt & Whitney Div.
West Palm Beach, FL 33402
Attn: Tech. Library (1)

United Technologies Corp.
Hamilton-Standard Div.
Windsor Locks, CT 06096
Attn: W. Ryan (1)

United Technologies Corp.
Sikorsky Aircraft Div.
Stratford, CT 06497
Attn: Tech. Library (1)

United Technologies Corp.
Research Laboratories
East Hartford, CT 06108
Attn: M. A. DeCresente (1)

United Technologies Corp.
Pratt & Whitney Aircraft Div.
E. Hartford, CT 06108
Attn: S. Bleckerman (1)

Westinghouse Electric Corp.
Research & Development Center
1310 Beulah Road
Pittsburgh, PA 15235
Attn: J. A. Cornie (1)

The Boeing Aerospace Co.
P. O. Box 3707
Seattle, WA 98124
Attn: T. J. Bosworth (1)

United Technologies Corp.
Hamilton-Standard Div.
Windsor Locks, CT 06096
Attn: W. A. Percival (1)

United Technologies Corp.
Research Laboratories
East Hartford, CT 06108
Attn: F. S. Galasso (1)

United Technologies Corp.
Research Laboratories
East Hartford, CT 06108
Attn: K. M. Prewo (1)

University of Tennessee
Space Institute
Tullahoma, TN 37388
Attn: M. A. Wright (1)

Whittaker Corp.
Research & Development Div.
3540 Aero Court
San Diego, CA 92123
Attn: Tech. Library (1)

Deposits & Composites, Inc.
318 Victory Drive
Herndon, VA 22070
Attn: J. C. Withers (1)

NASA-Lewis Research Center
21000 Brookpark Road
Cleveland, OH 44135
Attn: R. G. Barrows (34)